Resveratrol Improves Oxidative Stress and Protects Against Diabetic Nephropathy Through Normalization of Mn-SOD Dysfunction in AMPK/SIRT-1-Independent Pathway

Munehiro Kitada,[1] Shinji Kume,[2] Noriko Imaizumi,[1] and Daisuke Koya[1]

OBJECTIVE—Despite the beneficial effects of resveratrol (RSV) on cardiovascular disease and life span, its effects on type 2 diabetic nephropathy remain unknown. This study examined the renoprotective effects of RSV in db/db mice, a model of type 2 diabetes.

RESEARCH DESIGN AND METHODS—Db/db mice were treated with RSV (0.3% mixed in chow) for 8 weeks. We measured urinary albumin excretion (UAE), histological changes (including mesangial expansion, fibronectin accumulation, and macrophage infiltration), oxidative stress markers (urinary excretion and mitochondrial content of 8-hydroxy-2'-deoxyguanosine [8-OHdG], nitrotyrosine expression), and manganese-superoxide dismutase (Mn-SOD) activity together with its tyrosine-nitrated modification and mitochondrial biogenesis in the kidney. Blood glucose, glycated hemoglobin, and plasma lipid profiles were also measured. The phosphorylation of 5'-AMP activated kinase (AMPK) and expression of silent information regulator 1 (SIRT1) in the kidney were assessed by immunoblotting.

RESULTS—RSV significantly reduced UAE and attenuated renal pathological changes in db/db mice. Mitochondrial oxidative stress and biogenesis were enhanced in db/db mice; however, Mn-SOD activity was reduced through increased tyrosine-nitrated modification. RSV ameliorated such alterations and partially improved blood glucose, glycated hemoglobin, and abnormal lipid profile in db/db mice. Activation of AMPK was decreased in the kidney of db/db mice compared with db/m mice. RSV neither modified AMPK activation nor SIRT1 expression in the kidney.

CONCLUSIONS—RSV ameliorates renal injury and enhanced mitochondrial biogenesis with Mn-SOD dysfunction in the kidney of db/db mice, through improvement of oxidative stress via normalization of Mn-SOD function and glucose-lipid metabolism. RSV has antioxidative activities via AMPK/SIRT1 independent pathway. ***Diabetes*** **60:1–10, 2011**

Resveratrol (RSV; 3,5,4'-trihydroxystilbene) is reported to be beneficial in cardiovascular diseases (1) and renal diseases (2–4), including ischemic/reperfusion injury (5). The beneficial effects are thought to be due to its antioxidative properties because it is known as a robust scavenger of superoxide (O^{2-}), hydroxyl radicals, and peroxynitrite (6,7). Oxidative stress has been implicated in the pathogenesis of diabetic vascular complications, including nephropathy (8). The mitochondria are recognized as one of the major sources of reactive oxygen species (ROS) in diabetes (9), and they can also be damaged by ROS. Manganese-superoxide dismutase (Mn-SOD), which is an important antioxidative enzyme and mainly regulates ROS metabolism in the mitochondria, is one of the mitochondrial targets of ROS such as peroxynitrite, and thus its activity might become reduced with ROS exposure (10). Therefore, conditions that lead to Mn-SOD dysfunction could increase ROS production and hence induce tissue damage associated with diabetic nephropathy. However, it remains unclear whether mitochondrial oxidative stress associated with Mn-SOD dysfunction contributes to diabetes-induced renal injury, and whether RSV has any beneficial effects on mitochondrial status including oxidative stress and biogenesis in the kidney of type 2 diabetes.

Reduced mitochondrial biogenesis and function are found in insulin-resistant metabolic tissues including skeletal muscle, liver, and fat in association with the pathogenesis of type 2 diabetes (11). In addition to the scavenging of ROS, RSV enhances mitochondrial biogenesis through the 5'-AMP activated kinase (AMPK)/silent information regulator 1 (SIRT1) pathway in the muscle and liver, resulting in life span extension or improvement of high-fat diet–induced metabolic impairment such as obesity and insulin resistance (12–14). On the other hand, mitochondrial biogenesis can be induced in tissues not only by increased energy demands due to cold, exercise, and metabolic changes such as those induced by caloric restriction (15), but also by damage to mitochondria caused by oxidative stress (16–18) and hereditary disorders (19). Oxidative stress-induced mitochondrial biogenesis has also been reported in various tissues and cells (16–18), including the myocardium of an animal model of type 1 diabetes (20). There is little information on whether mitochondrial status including mitochondrial biogenesis is changed in the kidney of type 2 diabetes, and if so, how it is regulated and whether it is related to the pathogenesis of diabetic nephropathy.

From the [1]Division of Diabetes and Endocrinology, Kanazawa Medical University, Kahoku-Gun, Ishikawa, Japan; and the [2]Department of Medicine, Shiga University of Medical Science, Otsu, Shiga, Japan.
Corresponding author: Daisuke Koya, koya0516@kanazawa-med.ac.jp.
Received 19 March 2010 and accepted 1 December 2010.
DOI: 10.2337/db10-0386
This article contains Supplementary Data online at http://diabetes.diabetesjournals.org/lookup/suppl/doi:10.2337/db10-0386/-/DC1.

TABLE 1
Effects of RSV treatment on body weight, kidney weight, blood pressure, blood glucose, glycated hemoglobin, and lipid profiles in the four groups of mice. Glycated hemoglobin was measured using an ADAMS-HA8106 analyzer (ARKRAY, Kyoto, Japan). Serum insulin levels and urinary albumin excretion were measured with ELISA kits. Triglycerides, total cholesterol, and nonesterified fatty acid (NEFA) were measured using an L-type triglyceride H kit, cholesterol E-test kit, and NEFA C-test kit, respectively

	db/m	db/m+RSV	db/db	db/db+RSV
n	19	17	19	18
Body weight (g)	29.0 ± 2.31	28.6 ± 1.32	49.3 ± 2.70†	48.7 ± 1.92†
Right kidney weight (g)	0.196 ± 0.021	0.187 ± 0.012	0.233 ± 0.012†	0.217 ± 0.012‡§
Mean blood pressure (mmHg)	94.7 ± 5.30	94.9 ± 4.97	102.8 ± 6.56†	100.5 ± 5.18‖
Fasting blood glucose (mg/dL)	92.75 ± 4.18	90.63 ± 5.76	314.63 ± 50.72†	264.75 ± 44.17 †¶
Fasting serum insulin (ng/mL)	2.81 ± 1.54	2.88 ± 0.65	8.21 ± 3.59†	4.40 ± 1.44 †, #
*Random-fed blood glucose (mg/dL)	121.4 ± 28.50	117.6 ± 29.36	503.4 ± 64.80†	426.9 ± 90.52 †, **
Glycated hemoglobin (%)	3.66 ± 0.36	3.73 ± 0.31	8.7 ± 1.08†	7.78 ± 0.46 †, ††
Total cholesterol (mg/dL)	60.9 ± 8.12	62.2 ± 7.29	122.2 ± 22.84†	124.0 ± 22.03†
Triglyceride (mg/dL)	71.9 ± 20.9	65.4 ± 22.0	205.3 ± 52.10††	126.6 ± 58.07‡‡
Free fatty acids (mEq/L)	0.48 ± 0.128	0.48 ± 0.114	1.165 ± 0.275††	0.954 ± 0.196††
Urinary albumin excretion (μg/day)	44.56 ± 21.62	34.74 ± 20.37	382.99 ± 159.02††	189.00 ± 67.87‡‡

Data are means ± SD. *Random-fed blood glucose levels were measured at 9–10 A.M. †$P < 0.001$ vs. db/m, db/m+RSV. ‡$P < 0.05$ vs. db/m, db/db. §$P < 0.001$ vs. db/m+RSV. ‖$P < 0.05$ vs. db/m, db/m+RSV. ¶$P < 0.05$ vs. db/db. #$P < 0.01$ vs. db/db. **$P < 0.001$ vs. db/db. ††$P < 0.001$ vs. others, db/db. ‡‡$P < 0.01$ vs. db/m, db/m+RSV.

Thus, the aim of this study was to investigate the potential effects of RSV on mitochondrial oxidative stress associated with Mn-SOD dysfunction and mitochondrial biogenesis in the kidney of db/db mice. The results of the current study indicate that the enhanced mitochondrial biogenesis with Mn-SOD dysfunction induced by tyrosine nitration was observed in the diabetic kidney. Treatment with RSV resulted in the amelioration of these functional and histological abnormalities and mitochondrial biogenesis in the diabetic kidney, possibly by the attenuation of oxidative stress through scavenging of ROS, normalization of Mn-SOD dysfunction in an AMPK/SIRT1-independent mechanism, and partial improvement of glucose-lipid metabolism.

RESEARCH DESIGN AND METHODS

Materials and antibodies. Details of the materials and antibodies used in the current study are available in the Supplementary Data.

Animals. Male db/db mice and age-matched db/m mice were purchased from Clea Japan (Tokyo, Japan). At 9 weeks of age, mice were divided into four groups: db/m mice, db/db mice, db/m mice treated with RSV, and db/db mice treated with RSV. RSV was mixed (0.3%) with chow and administered orally. Body weight, blood glucose level, food consumption, and blood pressure were measured every 2 weeks in all animals. The blood pressure of conscious mice was measured at steady state by a programmable tail-cuff sphygmomanometer (BP98-A; Softron, Tokyo, Japan). At 17 weeks of age, individual mice were placed in metabolic cages for 24-h urine collection. The urine samples were stored at −80°C until analysis. Mice were anesthetized by intraperitoneal injection of pentobarbital sodium, and then the right kidneys were removed and stored at −80°C for experiments as described below. After collection of blood samples from the left cardiac ventricle, the left kidney was perfused with ice-cold phosphate-buffered saline (PBS) and 10% neutral buffered formalin and then removed. The Research Center for Animal Life Science of Kanazawa Medical University approved all experiments.

Morphological analysis and immunohistochemistry. To assess the mesangial expansion, thirty glomeruli, cut at the vascular pole, randomly selected from each mouse were measured the periodic acid/Schiff (PAS)-positive material in the mesangial area and glomerular tuft area by computer-assisted color image analysis (Micro Analyzer; Japan Poladigital, Tokyo, Japan) as previously described (21).

For semiquantitative evaluation of the fibronectin, F4/80 and nitrotyrosine scores, 20 randomly selected glomerulus or tubulointerstitial areas per mouse were graded in a double-blind manner, as reported previously (21–23), with minor modifications.

8-OHdG levels in mitochondrial DNA and quantification of mitochondrial DNA deletion mutation. The mitochondrial DNA (mtDNA) was extracted from the kidney using the mtDNA Extractor CT kit. The 8-OHdG levels in DNase I-digested mtDNA were determined by ELISA using a kit (8-OHdG Check, Institute for the Control of Aging, Shizuoka, Japan) (24). We assessed the deletion mutation, D-17, as reported previously (23). The sequences of primers are listed in Supplementary Table 1.

Detection of O^{2-} formation in renal isolated mitochondria. The mitochondria were isolated from the renal cortex of all groups of mice using the mitochondria isolation kit, according to the manufacturer's instructions. O^{2-} production from the mitochondria was measured by L-012 chemiluminescence (CL) dye (25). Mitochondrial suspensions were diluted to a final protein concentration of 0.1 mg/mL in 0.2 mL of PBS buffer containing 100 μmol/L L-012. O^{2-} from mitochondria was detected after stimulation with 4 mmol/L succinate and 20 μg/mL antimycin A by L-012. The CL registered at intervals of 30 s over 5 min with a chemiluminometer, and the signal was expressed as counts of CL/min/100 μg protein at 5 min. In ex vivo study, similar experiments were performed in isolated mitochondria from the renal cortex of db/db mice at various concentrations (10^{-3}–100 μmol/L) of RSV or 100 U/mL SOD. In addition, O^{2-} from the reaction of hypoxanthine and xanthine oxidase was also measured. L-012 (100 μM) was incubated for 5 min in PBS buffer containing 100 μmol/L diethylenetriamine pentaacetic acid (DTPA) and 1 mmol/L hypoxanthine at room temperature, and then the basal (background) signal was determined in a chemiluminometer at intervals of 30 s for 5 min. The CL was counted after the addition of 10 mU/mL xanthine oxidase at various concentrations of RSV (10^{-3}–100 μmol/L) or 100 U/mL SOD at intervals of 30 s over 5 min.

Mn-SOD activity. The whole kidney was homogenized in 2 mL of 50 mmol/L Tris HCl buffer containing 0.1 mmol/L ethylenediaminetetraacetic acid (EDTA) at pH 7.0. After centrifugation at 15,000*g* for 15 min, the supernatant was removed and total protein concentration was measured using a protein assay kit. The Mn-SOD activity was measured by inhibiting extracellular and cytosolic Cu/Zn SOD activity with KCN (1 mmol/L) using an SOD assay kit (WST-1) (26). One unit of SOD activity was defined as the amount causing 50% inhibition of the initial rate of reduction of WST-1 (2-(4-Iodophenyl)-3-(4-nitrophenyl)-5-(2, 4-disulfophenyl)-2H-tetrazolium, monosodium salt), a highly water-soluble tetrazolium salt. Mn-SOD activity was calculated in terms of protein content (U/μg) and expressed as a fold increase relative to that found in db/m mice.

Immunoprecipitation and Western blot analysis. The whole kidney was homogenized in ice-cold radioimmunoprecipitation assay buffer. Solubilized protein (1 mg) was used for immunoprecipitation with rabbit polyclonal anti–Mn-SOD antibody (10 μg/mL) using protein A Sepharose, and then Western blot analysis was performed with mouse monoclonal antinitrotyrosine antibody (1:1000) or rabbit polyclonal anti–Mn-SOD antibody (1:1000). Samples of protein solutions from the kidney were used for Western blotting with anti-phospho-AMPKα (Thr172) antibody, anti-AMPKα (23A3) antibody (1:1000), or anti-SIRT1 antibody (1:1000).

Quantitative real-time PCR. Isolation of total RNA from kidney, and determination of complementary DNA synthesis by reverse transcription and quantitative real-time PCR were performed as described previously (23). PCR primer sets are listed (Supplementary Table 1).

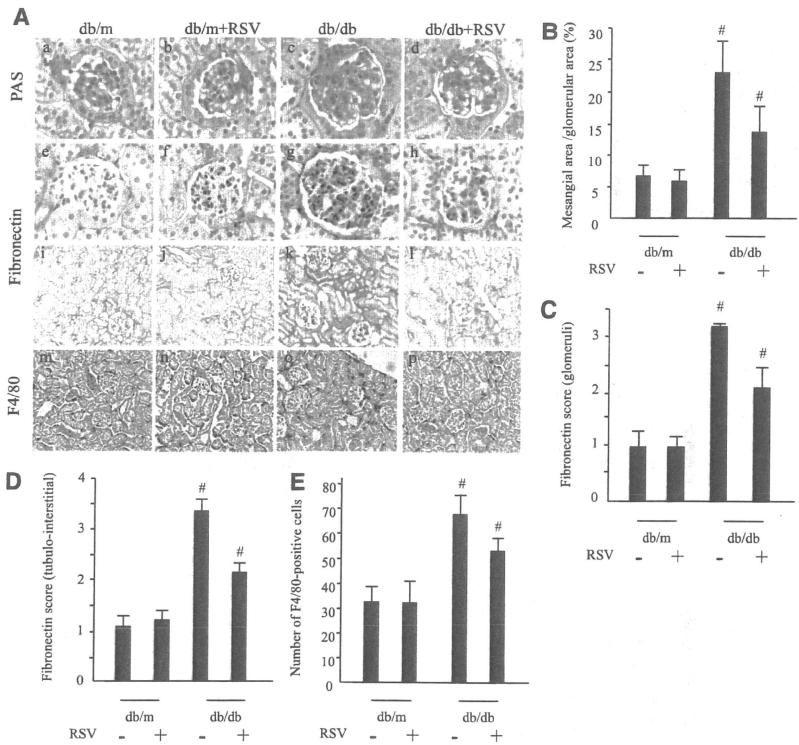

FIG. 1. Treatment with RSV ameliorates the mesangial matrix expansion in db/db mice. *A*: Representative photomicrographs of PAS-stained kidney (a–d). Data are results of independent experiments in each group with six mice per group. Original magnification: ×400. Treatment with RSV reduced glomerular and interstitial fibronectin accumulation and the number of F4/80-positive cells in db/db mice. Representative photomicrographs of immunohistochemistry for glomerular fibronectin (e–h), interstitial fibronectin (i–l), and F4/80 (m–p). Data are the results of independent experiments in each group with three to five mice per group. Original magnification, ×400 for glomerular fibronectin, ×200 for interstitial fibronectin, and ×100 for F4/80 staining. *B*: Quantitative assessment of the mesangial matrix area. Data are means ± SD (n = 6, #P < 0.01 vs. other groups). *C–E*: Quantitative assessment of fibronectin and F4/80 staining. Data are means ± SD (n = 3–5, #P < 0.01 vs. other groups).

Cell culture. Murine proximal tubular cells (mProx) (derivative, patent WO9927363, Japan, U.S., European Union), kindly provided by CMIC Co., were cultured as described previously (27).

Retroviral infection. The pSUPERretro and pSUPERretro-SIRT1 RNA interference vectors were kind gifts from Dr. L. Guarente (Massachusetts Institute of Technology, Cambridge, MA). Human embryonic kidney 293T cells were transfected with pSUPERretro or pSUPERretro-SIRT1 RNAi by using Lipofectamine reagent. At 48 h after transfection, the media containing the retroviruses were collected, centrifuged, and transferred to mProx treated by polybrene (1 g/mL). The infected cells were selected by treatment with puromycin (2.5 μg/mL) for several days as described previously (28).

Infection of adenoviral dominant negative-AMPK. Adenoviruses containing green fluorescent protein (Ad-GFP) or dominant-negative AMPK (DN-AMPK) were added to subconfluent mProx at a concentration of 50 multiplicity of infection for 1 h at 37°C in serum-free Dulbecco's modified Eagle's medium (29).

Detection of ROS in mProx. To determine the effect of RSV on oxidative stress in mProx, cells were incubated with RSV (10 μmol/L) for 180 min at 37°C before exposure to H_2O_2 (10 μmol/L). After incubation, the levels of intracellular ROS were measured with the fluoroprobe 2.7-dichlorodihydrofluorescein diacetate. The intracellular ROS was evaluated as the fluorescence intensity (an excitation wavelength 488 nm, an emission wavelength 525 nm) of dichlorofluorescein by Infinite M200 microplate reader (Tecan Japan Co., Kanagawa, Japan). The results of intracellular ROS are expressed in arbitrary units.

mtDNA content. Well-conserved nuclear and other mitochondrial genes were selected to quantify mtDNA copy number per nuclear genome. Cytochrome c oxidase subunit 2 was used as a marker for mtDNA and uncoupling protein 2 for nuclear DNA. Renal DNA was extracted from frozen kidney tissues of all animals using the DNeasy tissue kit. Total DNA concentration was determined using a PicoGreen DNA quantitation kit. Specific mouse primer sequences are provided in the Supplementary Table 1. mtDNA per nuclear genome was calculated as the ratio of cytochrome c oxidase subunit 2 DNA to uncoupling protein 2 DNA (30) and expressed as the fold increase relative to that found in db/m mice.

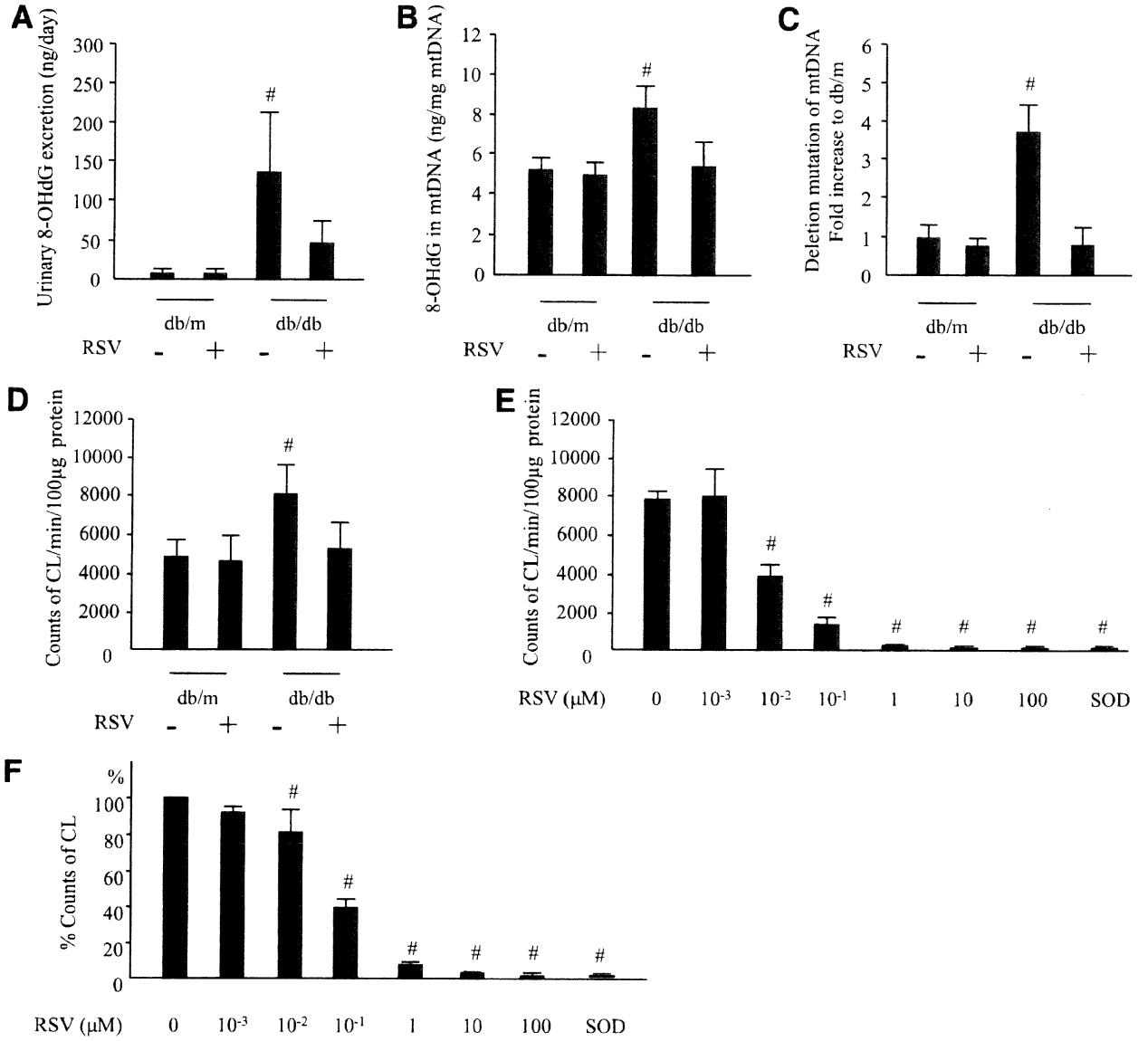

FIG. 2. RSV suppresses oxidative damage in db/db mice, and RSV scavenges O^{2-} production from mitochondria. *A*: Urinary 8-OHdG excretion for 24 h was measured. Data are means ± SD (n = 9–11, #P < 0.05 vs. other groups). *B*: 8-OHdG contents in mtDNA of the kidney samples were measured. Data are means ± SD (n = 3–4, #P < 0.05 vs. db/m mice group). *C*: Frequencies of deletion mutation of mtDNA in the kidney were determined by quantitative PCR method. Data are means ± SD (n = 3–4, #P < 0.05 vs. other groups). *D*: O^{2-} production from renal isolated mitochondria by stimulation with succinate and antimycin A was determined in all groups. O^{2-} production was expressed as counts of CL per 100 μg protein. Data are means ± SD (n = 8, #P < 0.05 vs. db/m mice group). *E*: O^{2-} production in mitochondria isolated from the kidneys of db/db mice by stimulation with succinate and antimycin A was measured in RSV at various concentrations (10^{-3}–100 μmol/L) or SOD (100 U/mL). O^{2-} production was expressed as counts of CL per 100 μg protein. Data are means ± SD (n = 8, #P < 0.01 vs. control [0]). *F*: O^{2-} production from the reaction of hypoxanthine/xanthine oxidase was measured in RSV at various concentrations (10^{-3}–100 μmol/L) or SOD (100 U/mL). The inhibitory effect of RSV against O^{2-} on this reaction was expressed as % counts of CL. Data are means ± SD (n = 4, #P < 0.01 vs. control [0]).

Citrate synthase activity. Citrate synthase activity in the kidney was determined using the citrate synthase activity measurement kit, according to the manufacturer's instructions.

Electron microscopy. The mitochondria in proximal tubular cells were observed by electron microscopy as previously described (23). Mitochondrial area and number were estimated in 15–18 micrographs, which were taken for renal proximal tubular cells of three animals of each group (20). The mitochondrial area was measured using the Image J software, and the number of mitochondria per cell was counted manually by a blind observer.

Statistical analysis. Data are expressed as means ± SD. The Tukey multiple-comparison test was used to determine the significance of pairwise differences among three or more groups. P < 0.05 was considered significant.

RESULTS

Characteristics of experimental mice. Table 1 details the characteristics of four groups of mice at the end of the experimental period. The whole body and right kidney weights were significantly higher in db/db mice compared with db/m mice. The mean blood pressure (MBP) was significantly higher in db/db mice than in db/m mice. RSV did not affect changes in MBP. Db/db mice exhibited markedly elevated blood glucose levels compared with db/m mice throughout the entire experiment. In db/db mice, treatment with RSV induced a partial improvement in blood glucose levels and glycated hemoglobin by the end

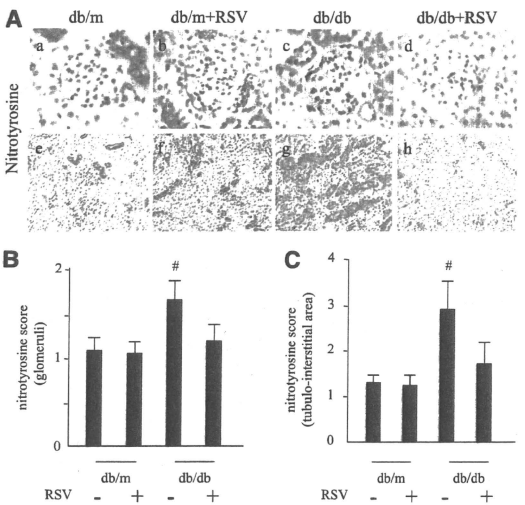

FIG. 3. Treatment with RSV suppresses diabetes-induced nitrotyrosine staining in the mouse kidney. *A*: Representative photomicrographs of renal nitrotyrosine expression. Data are results of independent experiments in each group with six mice per group. Original magnification: ×400 for glomerular nitrotyrosine (a–d) and ×100 for tubulointerstitial nitrotyrosine (e–h) staining. *B* and *C*: Semiquantitative scores for nitrotyrosine in glomerular and tubulointerstitial lesions. Data are means ± SD (n = 6, #P < 0.05 vs. other groups).

Q:7

of the experiments. Serum lipid profiles including total cholesterol, triglyceride, and free fatty acid levels were also significantly elevated in db/db mice compared with db/m mice; the increases in triglycerides and free fatty acids were partially rescued by RSV (Table 1). In addition, an impairment of glucose and insulin tolerance was evident in db/db mice relative to db/m mice (Supplementary Fig. 1), and high levels of fasting glucose and insulin (Table 1) indicating insulin resistance were also observed in db/db mice. Such alteration of insulin resistance in db/db mice was partially improved by treatment with RSV. There were no differences in body weight and food consumption between untreated and RSV-treated db/db mice. The 24-h urine volume was significantly larger in db/db mice compared with db/m mice, and this was partially reduced by treatment with RSV (data not shown).

Changes in urinary albumin excretion. To evaluate the effects of RSV on functional abnormalities in db/db mice, we measured the urinary albumin excretion. Values were markedly higher in db/db mice and RSV treatment significantly reduced urinary albumin excretion (Table 1), indicating that RSV ameliorates the functional abnormality of diabetic nephropathy in db/db mice.

Changes in kidney morphology. Figure 1*A* a–d shows representative photomicrographs of mesangial matrix accumulation in the PAS-stained kidneys of the four groups. The mesangial matrix was more extensive in the glomeruli of db/db mice than in db/m mice, and treatment with RSV reduced such expansion. Figure 1*B* shows the results of quantitative analysis of mesangial matrix expansion in all groups. Although the ratio of mesangial matrix/glomerular area was markedly larger in db/db mice than in db/m mice, treatment with RSV significantly reduced this expansion.

Immunohistochemistry for fibronectin (Fig. 1*A* e–h and i–l) also showed a significantly higher score for renal glomerular and tubulointerstitial expression in db/db mice than in db/m mice (Fig. 1*C* and *D*). Treatment with RSV reduced the score for fibronectin in db/db mice but had no effect on db/m (Fig. 1*C* and *D*).

The number of cells positive for F4/80 (a macrophage marker) in the renal interstitial lesion was significantly higher in db/db mice than in db/m mice (Fig. 1*A* m–p), but this pattern was not found in the glomeruli (data not shown). Treatment with RSV reduced the number of F4/80-positive cells in the renal interstitial lesions of db/db mice (Fig. 1*E*). These results indicate that RSV might improve glomerular and interstitial histological abnormalities including mesangial expansion, fibronectin accumulation and increased interstitial macrophage infiltration in the kidney of db/db mice.

Changes in urinary 8-OHdG excretion and mitochondrial oxidative damage in the kidney. Urinary 8-OHdG excretion was markedly higher in db/db mice compared with db/m mice but diminished after treatment with RSV (Fig. 2*A*). The 8-OHdG content (Fig. 2*B*) and subsequent deletion mutation (Fig. 2*C*) in the mtDNA isolated from the kidneys of db/db mice were significantly higher than in db/m mice. These mitochondrial alterations in mtDNA were not observed in the kidney of db/db mice treated with RSV. In addition, O^{2-} production from the isolated renal mitochondria after stimulation with succinate and antimycin A was significantly increased in db/db mice, but treatment with RSV restored it to normal in db/db mice. In ex vivo

experiments, the addition of RSV exogenously attenuated the levels of O^{2-} from the renal mitochondria of db/db mice in a dose-dependent manner (Fig. 2*D*). Moreover, RSV could also scavenge O^{2-} production from reaction of hypoxanthine and xanthine oxidase in a dose-dependent manner. These results suggest that the enhancement of both systemic oxidative damage and renal mitochondrial oxidative damage was observed in db/db mice and that RSV has antioxidative activity.

Changes in nitrotyrosine expression in the kidney. Figure 3*A* a–h show representative immunohistochemical staining for nitrotyrosine in the kidney. The semiquantitative scores for nitrotyrosine in both the glomerular and the tubulointerstitial lesions of the renal cortex were increased in db/db mice compared with those of db/m mice (Fig. 3*B* and *C*). Treatment with RSV reduced the scores in the glomeruli and tubulointerstitium of db/db mice but had no effect on the lesions of db/m mice (Fig. 3*B* and *C*). These results indicate that tyrosine nitration of proteins is enhanced in the kidney of db/db mice and that RSV seems to attenuate the effect.

Changes in Mn-SOD expression and activity in the kidney. The mRNA and protein expression of Mn-SOD was higher in db/db mice than in db/m mice (Fig. 4*A–C*). The Mn-SOD activity was significantly lower in the kidney of db/db mice compared with that of db/m mice (Fig. 4*D*). Nitrotyrosine immunoreactivity was significantly higher in Mn-SOD immunoprecipitates from the kidney of db/db mice than in that from db/m mice, and the increase in immunoreactivity was attenuated by treatment with RSV in db/db but not db/m mice (Fig. 4*E* and *F*). These findings suggest that Mn-SOD activity could be reduced by modifying tyrosine nitration in the kidneys of db/db mice.

mRNA levels of mitochondrial biogenesis–related genes and the enzyme activity of citrate synthase. To evaluate mitochondrial biogenesis, we assessed peroxisome proliferator-activated receptor γ coactivator (PGC)-1α, nuclear respiratory factor (NRF)-1, and cytochrome c oxidoreductase mRNA expression levels and mtDNA contents in the kidney. The citrate synthase activity was also measured in the kidney. All these were significantly higher in the kidneys of db/db mice than in that of db/m mice (Fig. 5*A–E*). These changes improved following treatment with RSV, consistent with the observed normalization of Mn-SOD activity and oxidative stress.

Electron microscopy. To confirm the beneficial effects of RSV on mitochondrial biogenesis, we examined the renal morphology in more detail by electron microscopy. The number and area of the mitochondria were significantly

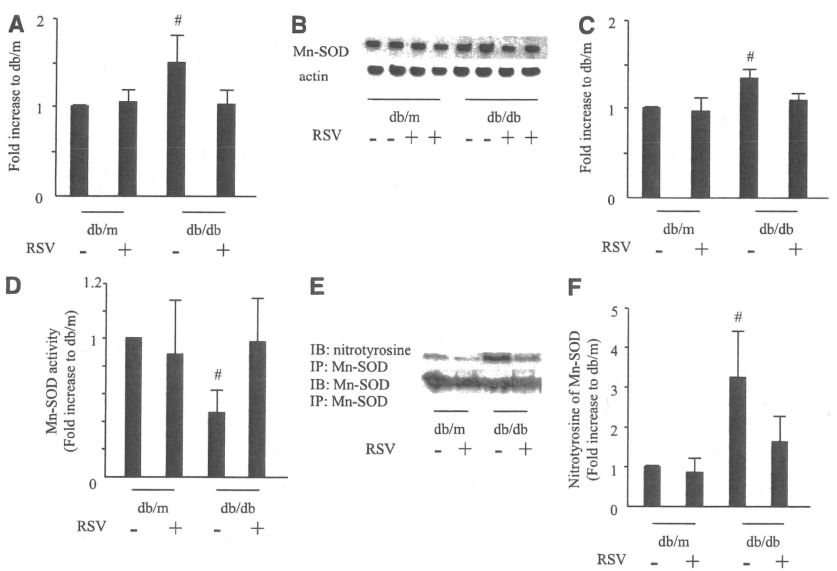

FIG. 4. Mn-SOD expression and activity in the kidney. *A*: **Mn-SOD mRNA expression in kidneys was quantified by real-time PCR and expressed as fold increase relative to db/m mice. Data are means ± SD (n = 9–11, #P < 0.05 vs. other groups).** *B*: **Mn-SOD protein expression in the kidney shown by representative immunoblots of Mn-SOD in protein extracts from the kidneys of mice of each group. Actin was loaded as an internal control.** *C*: **Quantitative analysis of Mn-SOD protein expression in the kidneys. Data are means ± SD (n = 4, #P < 0.05 vs. other groups).** *D*: **Mn-SOD activity in the kidney homogenate is expressed as fold increase compared with db/m mice. Data are means ± SD (n = 9–11, #P < 0.05 vs. other groups). Immunoreactivity to nitrotyrosine for immunoprecipitated Mn-SOD. Proteins from the kidneys of each group were immunoprecipitated with anti–Mn-SOD antibodies and blotted for nitrotyrosine antibodies. Representative results of Western blotting are shown (*E*), and the ratio to immunoprecipitated Mn-SOD is shown (*F*). Data are means ± SD (n = 6, #P < 0.05 vs. other groups).**

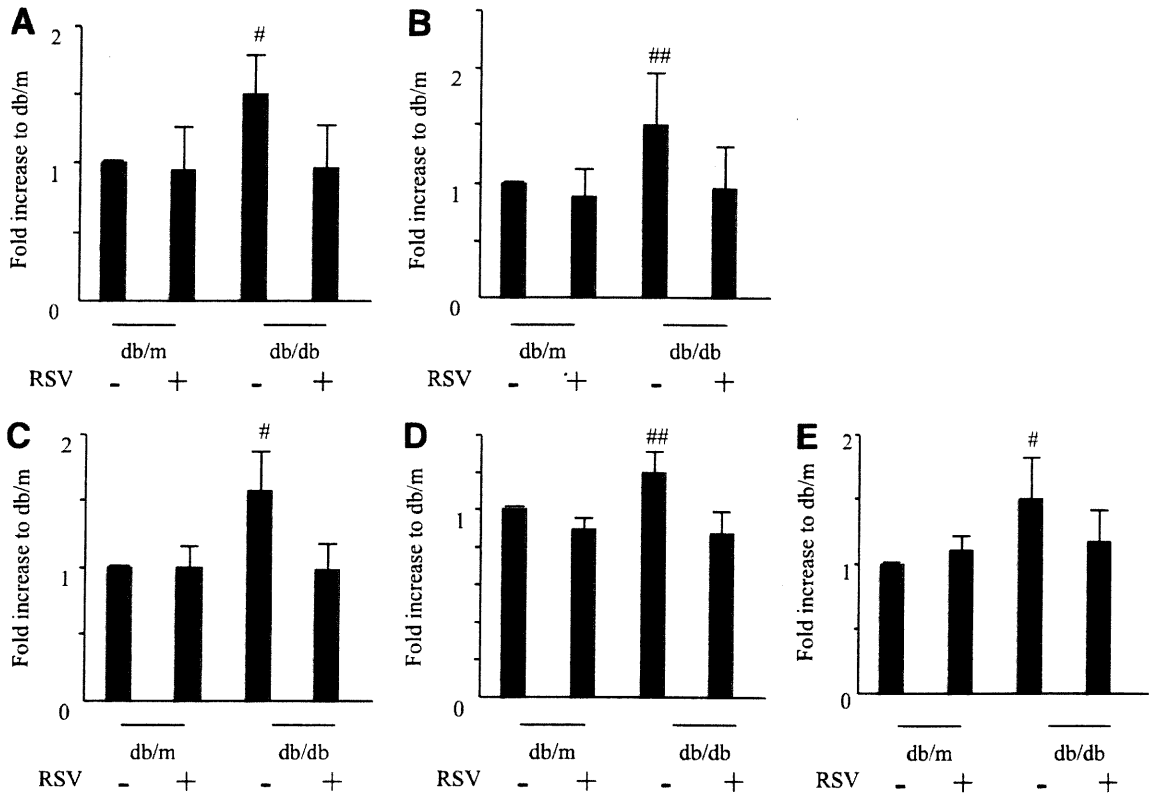

FIG. 5. PGC-1α, NRF-1, and cytochrome c oxidoreductase mRNA expression levels, mtDNA contents, and the enzyme activity of citrate synthase in the kidney. The mRNA expression levels of PGC-1α (*A*), NRF-1 (*B*), cytochrome c oxidoreductase (*C*), and mtDNA contents (*D*) were quantified by real-time PCR and expressed as fold increases from db/m mice. Data are means ± SD (n = 9–11, mRNA expression, n = 6–8; mtDNA content, #P < 0.05 vs. other groups, ##P < 0.01 vs. other groups). *E*: The citrate synthase activity was measured in the kidney of all groups. Data are means ± SD (n = 8, #P < 0.05 vs. other groups).

larger in renal proximal tubular cells of db/db mice compared with db/m mice, but treatment with RSV rescued these differences in db/db mice (Fig. 6*A–C*).

Changes in AMPK activation and SIRT 1 expression in the kidney. We assessed whether RSV activates AMPK in the kidney using immunoblotting for phosphorylation of AMPK. Activation of AMPK was significantly reduced in the kidney of db/db mice compared with db/m mice, and RSV did not alter AMPK activation in the kidney (Fig. 7*A* and *B*). In addition, SIRT1 expression was no different among the groups (Fig. 7*A* and *C*).

RSV exerts antioxidative effects in AMPK/SIRT1-independent mechanism in cultured renal proximal tubular cells. RSV attenuated intracellular ROS in both the SIRT1-knocked-down and DN-AMPK–overexpressing renal proximal tubular cells as well as in control cells. These results indicate that RSV exerts antioxidative effects independent of the AMPK/SIRT1 pathway (Fig. 7*D* and *E*).

DISCUSSION

In this study, we showed the potential benefits of RSV in ameliorating the renal injury and the enhanced mitochondrial biogenesis with Mn-SOD dysfunction observed in the diabetic kidney. We also demonstrated that RSV seems to exert these effects by improving the oxidative stress status in the kidney via the scavenging of ROS, normalization of Mn-SOD dysfunction, and partial rescue of glucose-lipid metabolism. Also, such antioxidative effects of RSV could be exerted in an AMPK/SIRT1–independent mechanism.

First, we showed that RSV improved renal functional and histological abnormalities such as albuminuria, mesangial expansion, glomerular and interstitial fibronectin accumulation, and interstitial macrophage infiltration in the kidney of db/db mice, a type 2 diabetes animal model. Oxidative stress has been implicated in the pathogenesis of diabetic nephropathy, and high glucose-induced ROS in renal mesangial or tubular cells contribute to overproduction of extracellular matrix proteins and inflammation (31,32). Because it has been reported that RSV is a robust scavenger of ROS (6,7), we assessed whether RSV has beneficial effects against diabetes-induced systemic and renal oxidative stress by measuring urinary 8-OHdG excretion and renal immunostaining for nitrotyrosine. Moreover, not only are mitochondria an important source of ROS, but also they themselves can be damaged by ROS. Therefore, we also assessed renal mitochondrial oxidative stress by measuring accumulation of mitochondrial 8-OHdG and D-17 deletion of mtDNA, which have been observed in diabetic nephropathy (33) and aging (24). In the current study, renal nitrotyrosine expression and mitochondrial oxidative damage indicated systemic, renal and particularly mitochondrial enhanced oxidative stress in the kidney of db/db mice, and there was clear attenuation of these markers following treatment with RSV. In addition, we showed that isolated mitochondrial O^{2-} production by stimulation with succinate and antimycin A was increased

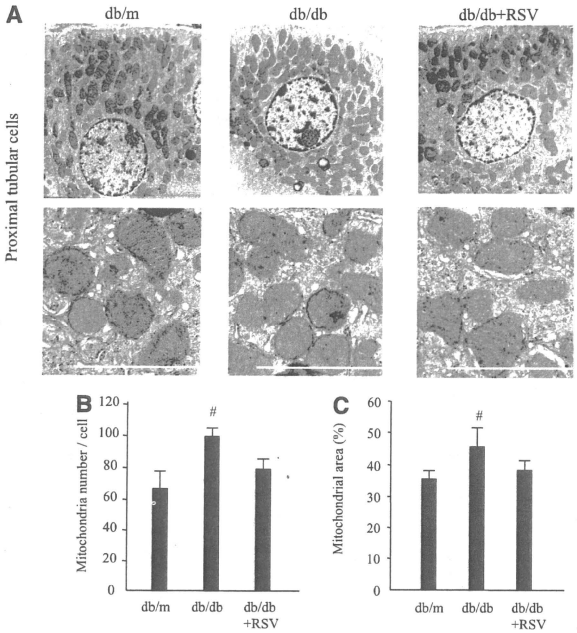

FIG. 6. Electron microscopy of kidney. *A*: Representative micrographs of proximal tubular cells from mice treated with RSV. Scale bar = 2 μm. Quantitative assessment of number (*B*) and area (*C*) of mitochondria in proximal tubular cells in mice treated with RSV. Data are means ± SD (n = 3, #P < 0.01 vs. other groups).

in db/db mice, and the RSV could scavenge ROS from the mitochondria.

The mitochondria are an important source of ROS in diabetes (9), and ROS metabolism in the mitochondria is mainly regulated by Mn-SOD, which is an important antioxidative enzyme in the mitochondria. In the diabetic state, high glucose- or FFA-induced overproduction of ROS from the mitochondria is inhibited by overexpression of Mn-SOD in vascular cells and tissues (9,34–37). Moreover, heterozygous Mn-SOD deficient mouse, which only have 50% of the Mn-SOD activity seen in wild-type mice, showed O^{2-}-induced mitochondrial oxidative damage (38), together with massive glomerulosclerosis, tubulointerstitial damage and inflammation including macrophage infiltration in the kidney (39). Therefore, regulation of ROS metabolism in the mitochondria via Mn-SOD function is an important protective factor in managing diabetic vascular complications including nephropathy. It is also known that tyrosine nitration at the active site of Mn-SOD is associated with reduction in enzymatic activity in the kidneys of several disease models (26,40–42). In the current study, we showed reduced Mn-SOD activity even when the expression of Mn-SOD was increased, and the former was probably caused by increased tyrosine nitration in the kidney of db/db mice. RSV might reduce tyrosine nitration of Mn-SOD and rescue the activation, resulting in improvement of mitochondrial oxidative stress and renal injury in diabetic kidney. Thus, RSV might ameliorate systemic, renal, and particularly mitochondrial oxidative stress in diabetes via the direct scavenging of ROS and normalization of the Mn-SOD function.

It has been reported recently that reduced mitochondrial biogenesis in insulin resistant tissues such as skeletal muscle, liver, or fat is associated with the pathogenesis of type 2 diabetes (11). In addition to its function as a ROS scavenger, several reports have implicated RSV in activating the AMPK/SIRT1 pathway to induce mitochondrial biogenesis (14), leading to life span prolongation and improvement of high-fat diet–induced metabolic impairment such as obesity and insulin resistance (12,13). We therefore examined mitochondrial biogenesis in the kidney based on mtDNA contents, mitochondria area and number, citrate synthase activity and overexpression of PGC-1α, NRF-1, cytochrome c oxidoreductase, and Mn-SOD. Interestingly, these factors were all enhanced in the kidney of db/db mice compared with db/m mice, and were rescued by RSV treatment, consistent with attenuation of systemic and renal mitochondrial oxidative stress including tyrosine nitration of Mn-SOD. Moreover, RSV did not alter AMPK activation or induction of Mn-SOD

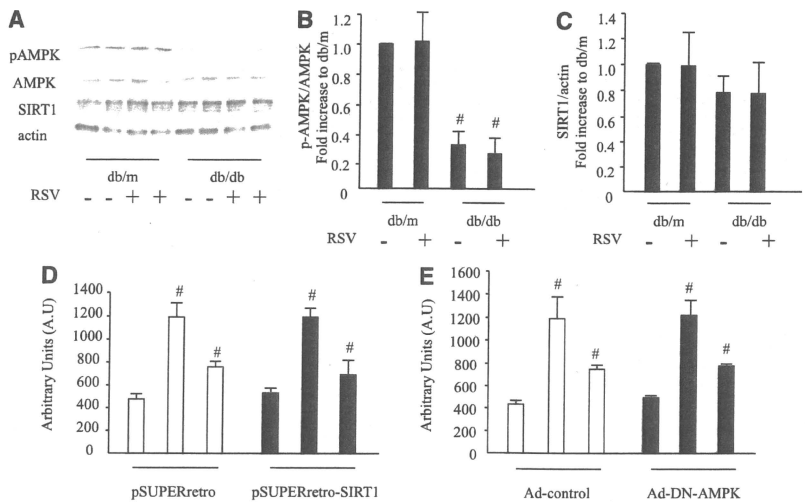

FIG. 7. AMPK activation and SIRT1 expression in the kidney and RSV attenuates ROS in both the SIRT1-knock down and the DN-AMPK–overexpressing renal mProx. *A*: Representative immunoblots of phospho-AMPKα (Thr172), AMPKα, and SIRT1 in protein extracts from the kidneys of mice of each group. Actin was loaded as an internal control. *B*: Quantitative analysis of phospho-AMPKα (Thr172). *C*: Quantitative analysis of SIRT1 protein expression. Data are means ± SD (n = 4, #P < 0.05 vs. db/m mice and db/m mice treated with RSV). *D*: Effects of RSV on the attenuation of oxidative stress in both the pSUPERretro and pSUPERretro-SIRT1 infected mProx exposed to H_2O_2. Data are means ± SD (n = 3, #P < 0.05 vs. other groups). *E*: Effects of RSV on the attenuation of oxidative stress in the adenovirus including GFP or DN-AMPK–overexpressing mProx exposed to H_2O_2. Data are means ± SD (n = 3, #P < 0.05 vs. other groups).

expression in the kidney. We also showed that RSV attenuated intracellular ROS in both the SIRT1 knocked-down and the DN-AMPK–overexpressing renal proximal tubular cells. These results suggest that systemic and/or renal mitochondrial oxidative stress contributes to the enhanced mitochondrial biogenesis in the kidney of the db/db mice and that RSV might improve mitochondrial biogenesis through the attenuation of oxidative stress, rather than through the activation of the AMPK/SIRT1 pathway. In this regard, Shen et al. (20) demonstrated that oxidative stress–induced mitochondrial biogenesis was increased in the myocardium of OVE26 diabetic mice as a possible compensatory reaction against oxidative stress–induced mitochondrial damage. Moreover, they showed that the myocardium-specific Mn-SOD transgenic mice crossed with OVE26 diabetic mice showed improvement of oxidant-induced mitochondrial biogenesis and dysfunction (37). Therefore, we suggest that the enhanced mitochondrial biogenesis in the kidney of db/db mice might also be a compensatory response to oxidative stress–induced mitochondrial damage; however further study is needed to elucidate the role of enhanced mitochondrial biogenesis associated with Mn-SOD dysfunction.

RSV has also been shown to reduce elevated blood glucose levels and metabolic impairment in diabetes, to be associated with mitochondrial biogenesis through the AMPK/SIRT1 activation pathway, as discussed above (12,13,43). In the current study, the elevated levels of glucose, glycated hemoglobin, triglycerides, and free fatty acids and impairment of glucose/insulin tolerance in db/db mice improved to some extent by treatment with RSV. It is therefore possible that RSV acts as an enhancer of mitochondrial biogenesis through AMPK/SIRT1 activation in liver and skeletal muscle, resulting in demonstrated improvements in abnormal glucose-lipid metabolism in db/db mice. In fact, we found that the phosphorylation of AMPK was reduced in the liver of db/db mice, and RSV could restore its alteration (data not shown). Therefore, RSV is likely exerting some of its effects via improvement of glucose homeostasis, and the systemic improvement of metabolism might at least in part contribute to the amelioration of renal oxidative stress and renal injury.

In conclusion, our study indicated that the enhanced mitochondrial biogenesis with Mn-SOD dysfunction by tyrosine nitration was observed in the diabetic kidney. RSV seems to improve these functional and histological abnormalities and ameliorate the enhanced mitochondrial biogenesis in diabetic kidney, possibly by attenuating the oxidative stress through scavenging of the ROS, by the normalization of the Mn-SOD dysfunction in an AMPK/SIRT1-independent mechanism, and by the partial improvement of the glucose and lipid metabolism.

ACKNOWLEDGMENTS

This work was supported by a Grant-in-Aid for Scientific Research (21591148) to D.K., and the grant from the Uehara Memorial Foundation to D.K.

No potential conflicts of interest relevant to this article were reported.

M.K. collected and analyzed the data and wrote the manuscript. S.K. collected and analyzed the data and contributed to discussion. N.I. collected and analyzed the data. D.K. contributed to discussion and reviewed and edited the manuscript.

The authors thank Yuki Tanaka for the technical support on fibronectin immunohistochemistry. They also thank Dr. Issa F.G., Word-Medex Pty Ltd. for help with preparing the manuscript.

REFERENCES

1. Bradamante S, Barenghi L, Villa A. Cardiovascular protective effects of resveratrol. Cardiovasc Drug Rev 2004;22:169–188
2. Do Amaral CL, Francescato HD, Coimbra TM, et al. Resveratrol attenuates cisplatin-induced nephrotoxicity in rats. Arch Toxicol 2008;82:363–370
3. Nihei T, Miura Y, Yagasaki K. Inhibitory effect of resveratrol on proteinuria, hypoalbuminemia and hyperlipidemia in nephritic rats. Life Sci 2001;68:2845–2852
4. Sharma S, Anjaneyulu M, Kulkarni SK, Chopra K. Resveratrol, a polyphenolic phytoalexin, attenuates diabetic nephropathy in rats. Pharmacology 2006;76:69–75
5. Sener G, Tuğtepe H, Yüksel M, Cetinel S, Gedik N, Yeğen BC. Resveratrol improves ischemia/reperfusion-induced oxidative renal injury in rats. Arch Med Res 2006;37:822–829
6. Leonard SS, Xia C, Jiang BH, et al. Resveratrol scavenges reactive oxygen species and effects radical-induced cellular responses. Biochem Biophys Res Commun 2003;309:1017–1026
7. Pervaiz S, Holme AL. Resveratrol: its biologic targets and functional activity. Antioxid Redox Signal 2009;11:2851–2897
8. Ceriello A. New insights on oxidative stress and diabetic complications may lead to a "causal" antioxidant therapy. Diabetes Care 2003;26:1589–1596
9. Nishikawa T, Edelstein D, Du XL, et al. Normalizing mitochondrial superoxide production blocks three pathways of hyperglycaemic damage. Nature 2000;404:787–790
10. MacMillan-Crow LA, Thompson JA. Tyrosine modifications and inactivation of active site manganese superoxide dismutase mutant (Y34F) by peroxynitrite. Arch Biochem Biophys 1999;366:82–88
11. Kim JA, Wei Y, Sowers JR. Role of mitochondrial dysfunction in insulin resistance. Circ Res 2008;102:401–414
12. Baur JA, Pearson KJ, Price NL, et al. Resveratrol improves health and survival of mice on a high-calorie diet. Nature 2006;444:337–342
13. Lagouge M, Argmann C, Gerhart-Hines Z, et al. Resveratrol improves mitochondrial function and protects against metabolic disease by activating SIRT1 and PGC-1alpha. Cell 2006;127:1109–1122
14. Um JH, Park SJ, Kang H, et al. AMP-activated protein kinase-deficient mice are resistant to the metabolic effects of resveratrol. Diabetes 2010;59:554–563
15. Liang F, Kume S, Koya D. SIRT1 and insulin resistance. Nat Rev Endocrinol 2009;5:367–373
16. Perez-de-Arce K, Foncea R, Leighton F. Reactive oxygen species mediates homocysteine-induced mitochondrial biogenesis in human endothelial cells: modulation by antioxidants. Biochem Biophys Res Commun 2005;338:1103–1109
17. Suematsu N, Tsutsui H, Wen J, et al. Oxidative stress mediates tumor necrosis factor-alpha-induced mitochondrial DNA damage and dysfunction in cardiac myocytes. Circulation 2003;107:1418–1423
18. Liu CS, Tsai CS, Kuo CL, et al. Oxidative stress-related alteration of the copy number of mitochondrial DNA in human leukocytes. Free Radic Res 2003;37:1307–1317
19. Heddi A, Stepien G, Benke PJ, Wallace DC. Coordinate induction of energy gene expression in tissues of mitochondrial disease patients. J Biol Chem 1999;274:22968–22976
20. Shen X, Zheng S, Thongboonkerd V, et al. Cardiac mitochondrial damage and biogenesis in a chronic model of type 1 diabetes. Am J Physiol Endocrinol Metab 2004;287:E896–E905
21. Koya D, Haneda M, Nakagawa H, et al. Amelioration of accelerated diabetic mesangial expansion by treatment with a PKC beta inhibitor in diabetic db/db mice, a rodent model for type 2 diabetes. FASEB J 2000;14:439–447
22. Deji N, Kume S, Araki S, et al. Structural and functional changes in the kidneys of high-fat diet-induced obese mice. Am J Physiol Renal Physiol 2009;296:F118–F126
23. Kume S, Uzu T, Horiike K, et al. Calorie restriction enhances cell adaptation to hypoxia through Sirt1-dependent mitochondrial autophagy in mouse aged kidney. J Clin Invest 2010;120:1043–1055
24. Kakoki M, Kizer CM, Yi X, et al. Senescence-associated phenotypes in Akita diabetic mice are enhanced by absence of bradykinin B2 receptors. J Clin Invest 2006;116:1302–1309
25. Daiber A, Oelze M, August M, et al. Detection of superoxide and peroxynitrite in model systems and mitochondria by the luminol analogue L-012. Free Radic Res 2004;38:259–269
26. Guo W, Adachi T, Matsui R, et al. Quantitative assessment of tyrosine nitration of manganese superoxide dismutase in angiotensin II-infused rat kidney. Am J Physiol Heart Circ Physiol 2003;285:H1396–H1403
27. Takaya K, Koya D, Isono M, et al. Involvement of ERK pathway in albumin-induced MCP-1 expression in mouse proximal tubular cells. Am J Physiol Renal Physiol 2003;284:F1037–F1045
28. Kume S, Haneda M, Kanasaki K, et al. SIRT1 inhibits transforming growth factor beta-induced apoptosis in glomerular mesangial cells via Smad7 deacetylation. J Biol Chem 2007;282:151–158
29. Kim SY, Jeoung NH, Oh CJ, et al. Activation of NAD(P)H:quinone oxidoreductase 1 prevents arterial restenosis by suppressing vascular smooth muscle cell proliferation. Circ Res 2009;104:842–850
30. Civitarese AE, Ukropcova B, Carling S, et al. Role of adiponectin in human skeletal muscle bioenergetics. Cell Metab 2006;4:75–87
31. Ha H, Lee HB. Reactive oxygen species as glucose signaling molecules in mesangial cells cultured under high glucose. Kidney Int Suppl 2000;77:S19–S25
32. Iglesias-De La Cruz MC, Ruiz-Torres P, Alcamí J, et al. Hydrogen peroxide increases extracellular matrix mRNA through TGF-beta in human mesangial cells. Kidney Int 2001;59:87–95
33. Kakimoto M, Inoguchi T, Sonta T, et al. Accumulation of 8-hydroxy-2′-deoxyguanosine and mitochondrial DNA deletion in kidney of diabetic rats. Diabetes 2002;51:1588–1595
34. Kiritoshi S, Nishikawa T, Sonoda K, et al. Reactive oxygen species from mitochondria induce cyclooxygenase-2 gene expression in human mesangial cells: potential role in diabetic nephropathy. Diabetes 2003;52:2570–2577
35. Munusamy S, MacMillan-Crow LA. Mitochondrial superoxide plays a crucial role in the development of mitochondrial dysfunction during high glucose exposure in rat renal proximal tubular cells. Free Radic Biol Med 2009;46:1149–1157
36. Kowluru RA, Atasi L, Ho YS. Role of mitochondrial superoxide dismutase in the development of diabetic retinopathy. Invest Ophthalmol Vis Sci 2006;47:1594–1599
37. Shen X, Zheng S, Metreveli NS, Epstein PN. Protection of cardiac mitochondria by overexpression of MnSOD reduces diabetic cardiomyopathy. Diabetes 2006;55:798–805
38. Williams MD, Van Remmen H, Conrad CC, Huang TT, Epstein CJ, Richardson A. Increased oxidative damage is correlated to altered mitochondrial function in heterozygous manganese superoxide dismutase knockout mice. J Biol Chem 1998;273:28510–28515
39. Rodriguez-Iturbe B, Sepassi L, Quiroz Y, Ni Z, Wallace DC, Vaziri ND. Association of mitochondrial SOD deficiency with salt-sensitive hypertension and accelerated renal senescence. J Appl Physiol 2007;102:255–260
40. van der Loo B, Labugger R, Skepper JN, et al. Enhanced peroxynitrite formation is associated with vascular aging. J Exp Med 2000;192:1731–1744
41. Cruthirds DL, Novak L, Akhi KM, Sanders PW, Thompson JA, MacMillan-Crow LA. Mitochondrial targets of oxidative stress during renal ischemia/reperfusion. Arch Biochem Biophys 2003;412:27–33
42. MacMillan-Crow LA, Crow JP, Kerby JD, Beckman JS, Thompson JA. Nitration and inactivation of manganese superoxide dismutase in chronic rejection of human renal allografts. Proc Natl Acad Sci USA 1996;93:11853–11858
43. Milne JC, Lambert PD, Schenk S, et al. Small molecule activators of SIRT1 as therapeutics for the treatment of type 2 diabetes. Nature 2007;450:712–716

Calorie restriction enhances cell adaptation to hypoxia through Sirt1-dependent mitochondrial autophagy in mouse aged kidney

Shinji Kume,[1,2] Takashi Uzu,[1] Kihachiro Horiike,[2] Masami Chin-Kanasaki,[1] Keiji Isshiki,[1] Shin-ichi Araki,[1] Toshiro Sugimoto,[1] Masakazu Haneda,[3] Atsunori Kashiwagi,[1] and Daisuke Koya[4]

[1]Department of Medicine and [2]Department of Biochemistry and Molecular Biology, Shiga University of Medical Science, Japan. [3]Department of Medicine, Asahikawa Medical College, Japan. [4]Division of Endocrinology and Metabolism, Kanazawa Medical University, Kahoku-Gun, Japan.

Mitochondrial oxidative damage is a basic mechanism of aging, and multiple studies demonstrate that this process is attenuated by calorie restriction (CR). However, the molecular mechanism that underlies the beneficial effect of CR on mitochondrial dysfunction is unclear. Here, we investigated in mice the mechanisms underlying CR-mediated protection against hypoxia in aged kidney, with a special focus on the role of the NAD-dependent deacetylase sirtuin 1 (Sirt1), which is linked to CR-related longevity in model organisms, on mitochondrial autophagy. Adult-onset and long-term CR in mice promoted increased Sirt1 expression in aged kidney and attenuated hypoxia-associated mitochondrial and renal damage by enhancing BCL2/adenovirus E1B 19-kDa interacting protein 3–dependent (Bnip3-dependent) autophagy. Culture of primary renal proximal tubular cells (PTCs) in serum from CR mice promoted Sirt1-mediated forkhead box O3 (Foxo3) deacetylation. This activity was essential for expression of Bnip3 and p27Kip1 and for subsequent autophagy and cell survival of PTCs under hypoxia. Furthermore, the kidneys of aged *Sirt1*$^{+/-}$ mice were resistant to CR-mediated improvement in the accumulation of damaged mitochondria under hypoxia. These data highlight the role of the Sirt1-Foxo3 axis in cellular adaptation to hypoxia, delineate a molecular mechanism of the CR-mediated antiaging effect, and could potentially direct the design of new therapies for age- and hypoxia-related tissue damage.

Introduction

Increasing age causes progressive postmaturational deterioration of tissues and organs, leading to impairment of tissue functioning, increased vulnerability to challenges, and death. The kidney is a typical target organ of age-associated tissue damage, and the increased incidence of chronic kidney disease (CKD) in the elderly is a health problem worldwide (1–3). However, there is little or no information on the mechanisms underlying age-associated kidney damage. Thus, studies designed to determine such molecular mechanisms could help formulate interventions that delay the onset and/or progression of CKD in elderly patients.

Among the several proposed theories on the pathogenesis of age-associated tissue damage, the mitochondrial ROS theory provides the basic mechanism of age-associated tissue dysfunction (4, 5): that age-dependent alteration in mitochondrial DNA (mtDNA) plays a fundamental role in the age-associated increase in ROS and subsequent tissue damage (6, 7). Further evidence linking alterations in mtDNA with progressive age-dependent tissue dysfunction can be found in individuals with mitochondrial genetic diseases and mice with deletion mutation of mtDNA, which display a phenotype that resembles premature aging, including kidney dysfunction (8, 9). Hypoxia is the cause of age-associated mitochondrial dysfunction (10) and is involved in age-dependent tissue damage affecting the brain (11), heart (12), and kidney (13). Furthermore, hypoxia modulates various cellular processes, such as apoptosis, cell cycle, autophagy, and glucose metabolism (14, 15). Elderly individuals suffer impairment of adaptation to systemic hypoxemia (16, 17); however, the molecular changes involved in age-associated cellular maladaptation to hypoxia are poorly understood.

Calorie restriction (CR) has various beneficial effects on health, including lifespan prolongation (18, 19). One mechanism of the beneficial effects of CR is attenuation of mitochondrial dysfunction in various pathological conditions (20, 21). Moreover, CR is suggested to affect cell adaptation to hypoxia (22), although the molecular mechanism of this effect remains elusive. In this context, uncovering the mechanism underlying CR-mediated attenuation of age-associated cellular and mitochondrial damage under hypoxia should contribute to the development of new therapies for age-associated tissue damage.

Studies on the mechanisms of CR-related longevity have identified the silent information regulator 2 (Sir2) as a survival factor that prolongs lifespan (23, 24). Sirt1, a mammalian homolog of Sir2, was originally identified as an NAD-dependent histone deacetylase (25). Recent studies have shown that Sirt1 is involved in the regulation of a wide variety of cellular processes, ranging from stress response, cell cycle, metabolism, and apoptosis in response to the cellular energy and redox status, through its deacetylase activity for more than 2 dozen known substrates (26). Thus, although Sirt1 is linked to CR-related longevity in model organisms (23, 24), the mechanism by which it extends lifespan in mammals and its role in age- or hypoxia-associated tissue damage remains unclear.

In the present study, we examined the mechanism of CR-related mitochondrial and cellular protection against hypoxia in aged mouse

Conflict of interest: The authors have declared that no conflict of interest exists.

Citation for this article: *J Clin Invest.* 2010;120(4):1043–1055. doi:10.1172/JCI41376.

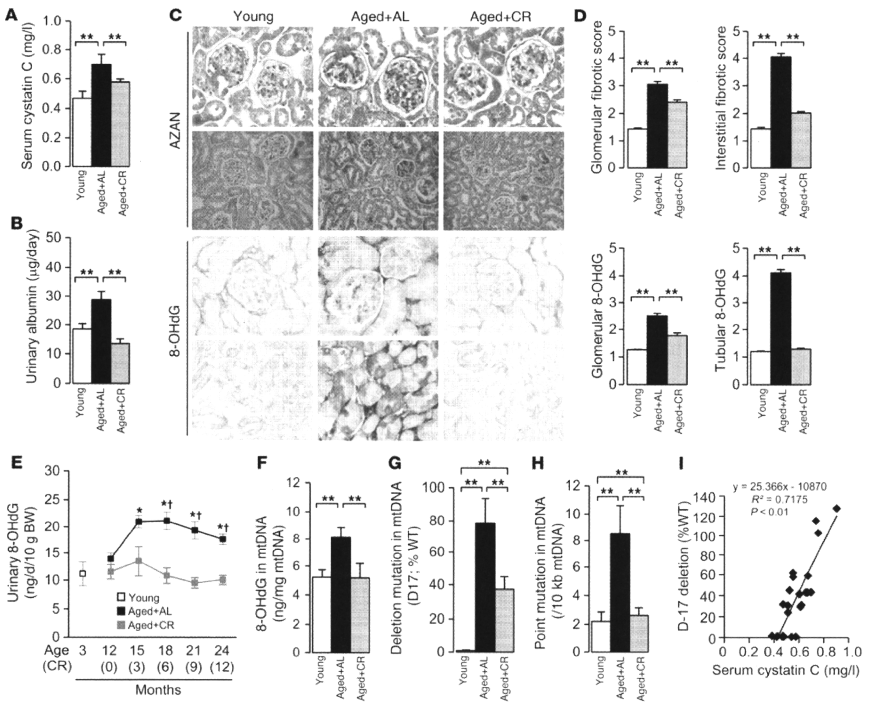

Figure 1

Effect of CR on mitochondrial oxidative damage in aged kidney. Experiments were performed on young mice or on aged mice subjected to AL or 12 months of CR. (**A** and **B**) Serum cystatin C levels (**A**) and 24-hour urinary albumin excretion levels (**B**) at the end of the experimental period. (**C**) Azan-stained and 8-OHdG–immunostained kidney sections. Original magnification, ×200 (Azan, bottom); ×400 (Azan, top, and 8-OHdG). (**D**) Quantitative analyses of Azan and 8-OHdG staining of glomerular and tubulointerstitial lesions. (**E**) Urinary 8-OHdG excretion levels during the observation period. Data are mean ± SEM. *$P < 0.05$ vs. young, †$P < 0.05$ vs. CR at the same time point. (**F**–**H**) 8-OHdG content (**F**), relative proportion of D-17 deletions (as percentage of WT; **G**), and frequencies of point mutations in cytochrome *b* gene (**H**) in mtDNA isolated from the kidney. Data are mean ± SEM. **$P < 0.05$. Each group includes 7–9 mice. (**I**) Correlation between D-17 prevalence and serum cystatin C level.

kidney, with a special focus on the role of Sirt1 on mitochondrial autophagy. The study identified a role for Sirt1 on cell adaptation to hypoxia, which provides what we believe to be a new molecular finding in CR-mediated antiaging effects, and shed light on the design of new therapies for age-related tissue damage including aged kidney.

Results

CR attenuates mitochondrial oxidative damage in aged kidney. First, we investigated whether adult-onset, long-term CR attenuates kidney damage and oxidative stress in aged mice. (Hereafter, unless otherwise indicated, *young* refers to mice 3 months of age and *aged* to mice 24 months of age.) During the 12-month experimental period, 3 aged mice of the ad libitum–fed (AL) group died as a result of malignancy and liver cirrhosis, whereas a single mouse of the CR group died as a result of malignancy (Supplemental Table 1; supplemental material available online with this article; doi:10.1172/JCI41376DS1). Significant differences were noted in various systemic metabolic parameters between the CR and AL mice (Supplemental Table 1). CR significantly inhibited age-associated increases in the renal dysfunction marker serum cystatin C, 24-hour urinary albumin excretion, and fibrotic changes in glomerular and interstitial lesions, with significantly reduced urinary excretion of the oxidative stress marker 8-OHdG (Figure 1, A–E). Significant accumulation of 8-OHdG was observed especially in the cytoplasm of the proximal tubular cells (PTCs) of AL mice, which was significantly attenuated by CR (Figure 1, C and D). In the kidneys of AL mice, accumulation of 8-OHdG in glomeruli was less than that in PTCs (Figure 1, C and D). Age-dependent

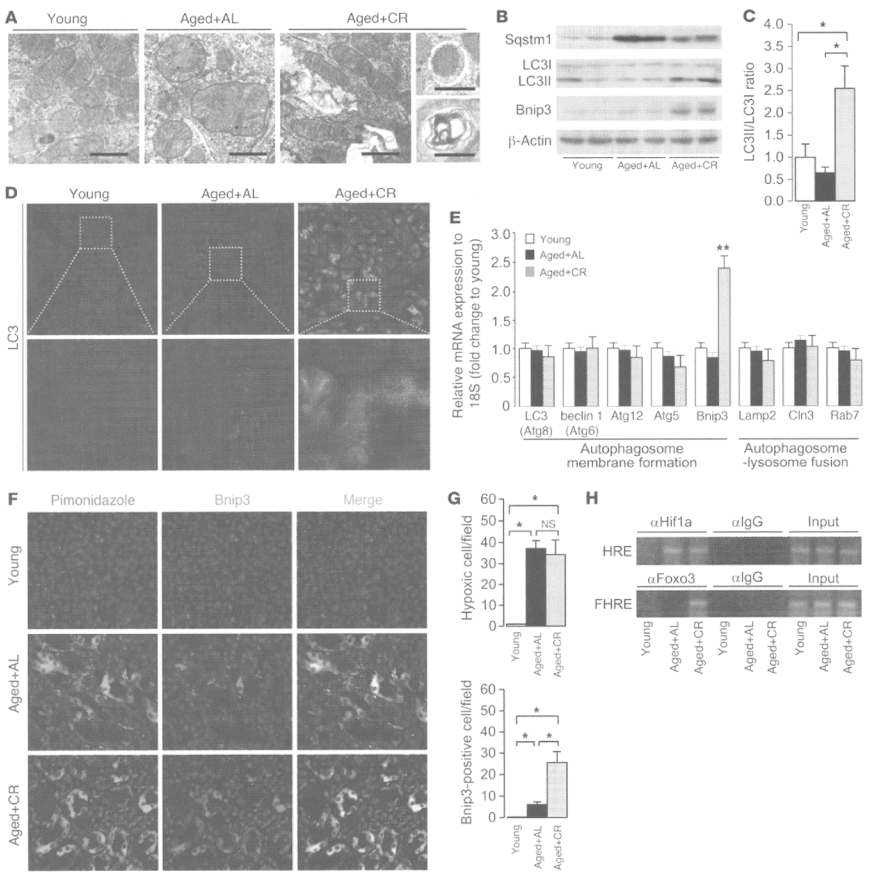

Figure 2

Effect of CR on Bnip3-mediated autophagy in aged kidney. (**A**) EM of representative renal PTCs. Scale bars: 1 μm. (**B**) IB analysis for autophagy-associated molecules. (**C**) Quantitative analysis of band intensity for LC3I and LC3II (ratio of LC3II to LC3I). (**D**) Immunofluorescent study for LC3 protein in the kidney. Original magnification, ×400 (top); ×1,000 (bottom). DAPI staining was performed as counterstaining. (**E**) mRNA expression associated with auto(lyso)phagosomal formation. Data are assessed as the ratio of mRNA expression of each molecule to mRNA expression of 18S ribosomal RNA and expressed as the fold change relative to the mean value of young mice. (**F**) Immunofluorescence study for pimonidazole and Bnip3 in the kidney. Original magnification, ×400. (**G**) Quantitative analysis of hypoxic pimonidazole$^+$ and Bnip3$^+$ cells per field in the kidney. (**H**) ChIP analysis to determine Hif1a and Foxo3 binding to Bnip3 promoter in the kidney samples. HRE, Hif-responsive element; FHRE, forkhead response element. Data are mean ± SEM. $^*P < 0.05$. $^{**}P < 0.05$ vs. other groups. Each group includes 7–9 mice.

increases in 8-OHdG accumulation as well as the major deletion mutation D-17 and point mutations in mtDNA are markers of age-associated mtDNA oxidative damage (27, 28). The age-associated mtDNA oxidative damages were significantly increased in the kidneys of AL mice and attenuated by CR (Figure 1, F–H). The prevalence of D-17 correlated significantly with serum cystatin C levels (Figure 1I), which suggests that mtDNA oxidative damage is related to age-dependent kidney dysfunction.

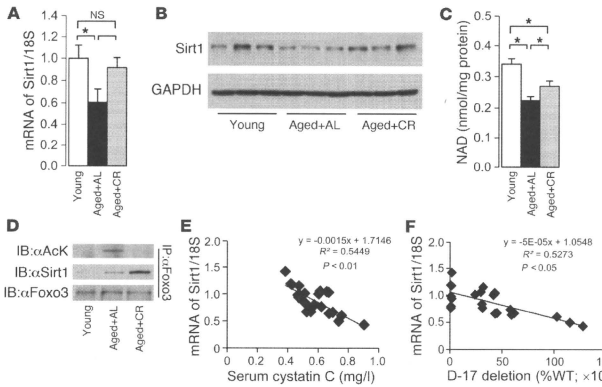

Figure 3
Effect of CR on Sirt1 activity in aged kidney. (**A** and **B**) mRNA (**A**) and protein (**B**) expression levels of Sirt1 in kidney samples. (**C**) NAD contents in kidney samples. (**D**) IP to detect acetylation of Foxo3 and interaction between Sirt1 and Foxo3 in kidney samples. Data are mean ± SEM. $^*P < 0.05$. Each group includes 7–9 mice. (**E**) Correlation between Sirt1 mRNA expression level and serum cystatin C level. (**F**) Correlation between Sirt1 mRNA expression level and D-17 prevalence.

CR enhances autophagy in aged kidney. EM analysis showed accumulation of senescent mitochondria in PTCs of AL mice, which exhibited swelling and disintegration of cristae (Figure 2A). Under normal circumstances, damaged mitochondria are degraded by autophagy, an intracellular process that allows the degradation of damaged proteins and organelles (29). In contrast to PTCs of AL mice, those of CR mice showed normal mitochondrial morphology with numerous auto(lyso)phagosomes (Figure 2A). Moreover, kidneys of AL mice contained higher levels of sequestosome 1 (Sqstm1; Figure 2B), a marker for in vivo impaired autophagy (30, 31). Lipidation of microtubule-associated protein 1 light chain 3 alpha (LC3), as assessed by the ratio of LC3I to LC3II conversion, as well as LC3 dots, which are known markers of enhanced autophagy (32, 33), were lower in AL mice than in CR mice (Figure 2, B–D). Thus, impaired autophagy might cause age-dependent mitochondrial oxidative damage in the kidney, and enhancement of autophagy could explain the CR-mediated mitochondrial protection.

CR enhances hypoxia-induced expression of BCL2/adenovirus E1B 19-kDa interacting protein 3 in aged kidney. We next analyzed the mRNA expression levels of various molecules involved in auto(lyso)phagosome formation (Figure 2E). Overexpression of BCL2/adenovirus E1B 19-kDa interacting protein 3 (Bnip3) mRNA was detected in CR mice (Figure 2E), and this was confirmed by IB (Figure 2B). Because Bnip3 is an initiator of hypoxia-induced autophagy (15, 34, 35), we examined the state of hypoxia and Bnip3 expression in the kidney. Pimonidazole® hypoxic cells were observed in PTCs of both AL and CR mice (Figure 2, F and G). Bnip3 expression was significantly enhanced in hypoxia-positive PTCs of CR mice, but it was less noted in AL mice (Figure 2, F and G). Bnip3 expression is positively regulated by certain transcriptional factors, including hypoxia-inducible factor 1 alpha (Hif1a) and forkhead box O3 (Foxo3) (15, 36). Chromatin IP (ChIP) indicated that Hif1a bound to Bnip3 promoter in the kidneys of both AL and CR mice, but Foxo3 bound to Bnip3 promoter only in CR mice (Figure 2H). These results suggest that Foxo3-mediated Bnip3 overexpression should be a molecular target for CR-mediated enhancement of hypoxia-induced autophagy in the aged kidney.

CR enhances Sirt1 activity in aged kidney. Because Foxo3 transcriptional activity is regulated by Sirt1 under certain conditions (37), we checked Sirt1 activity and its interaction with Foxo3. The mRNA and protein expression levels of Sirt1 were significantly decreased in the kidneys of AL mice and enhanced by long-term CR (Figure 3, A and B). NAD content in AL mice significantly decreased compared with that of young mice, but this decrease was attenuated by CR (Figure 3C). IP analysis revealed that Sirt1 interacted with and deacetylated Foxo3 in the kidney of CR mice, but not in AL mice (Figure 3D). Thus, Sirt1 activity was decreased in the aged kidney and enhanced by long-term CR. Furthermore, Sirt1 mRNA expression levels correlated negatively with serum cystatin C levels and prevalence of D-17 (Figure 3, E and F), which suggests that Sirt1 is associated with age-associated kidney dysfunction and mitochondrial damage.

Foxo3 is essential for CR-mediated enhancement of hypoxia-induced Bnip3 expression and autophagy. To investigate whether CR-dependent enhancement of hypoxia-induced Bnip3 expression and autophagy is reproducible in vitro, PTCs were incubated with serum from CR or AL rodents (20, 38, 39), and then exposed to hypoxia (1% O_2) for 24 hours. We reproduced a clear enhancement of hypoxia-induced Bnip3 expression as well as autophagy, as determined by LC3II formation and LC3 dots, in CR serum compared with AL serum (Figure 4, A–C). We confirmed that hypoxia failed to induce autophagy in Bnip3-knockdown cells (Supplemental Figure 1), which suggests that Bnip3 is essential for hypoxia-induced autophagy in PTCs. The siRNA for Foxo3 significantly inhibited CR-mediated enhancement of hypoxia-induced Bnip3 expression and autophagy (Figure 4, A–C). However, Foxo3 deficiency failed to inhibit hypoxia-induced autophagy in Bnip3-overexpressing PTCs under CR serum (Figure 4, D–F), which suggests that Foxo3 regulates hypoxia-induced autophagy through Bnip3 overexpression in CR serum.

Sirt1 is essential for CR-mediated enhancement of hypoxia-induced Bnip3 expression and autophagy. Retrovirally mediated Sirt1 knockdown significantly inhibited CR-mediated enhancement of hypoxia-induced Bnip3 expression and autophagy (Figure 5, A–C). Dominant-negative Sirt1 (H355A) lacking deacetylase activity inhibited hypoxia-induced autophagy under CR serum, whereas it failed to inhibit autophagy in Bnip3-overexpressing PTCs (Figure 5, D–F). Furthermore, Sirt1 overexpression did not affect Bnip3 knock-

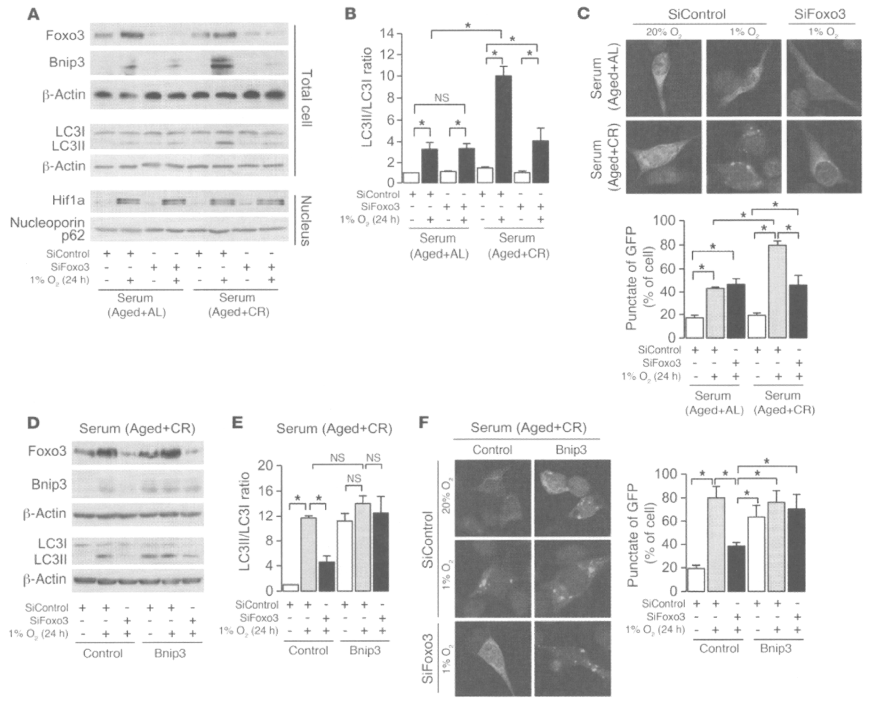

Figure 4

Involvement of Foxo3 on CR-mediated enhancement of autophagy under hypoxia. (**A**) Expression of Foxo3, autophagy-associated molecules, and nuclear Hif1a under hypoxia (1% O_2, 24 hours) in cells transfected with siRNA control or siRNA for Foxo3 under AL or CR serum. To detect LC3I and LC3II bands, cells were preincubated with lysosomal inhibitor (E64d and pepstatin A). (**B**) Quantitative analysis of the ratio of LC3II to LC3I ($n = 4$). (**C**) Hypoxia-induced autophagy in cells transfected with siRNA control or siRNA for Foxo3 in AL or CR serum. Autophagy was detected as dot spot of GFP-LC3 protein. Original magnification, ×400. Bottom: Percentage of GFP^+ cells with punctate GFP-LC3 fluorescence. (**D**) Expression of Foxo3 and autophagy-associated molecules under hypoxia in retrovirally mediated Bnip3-overexpressing cells transfected with siRNA control or siRNA for Foxo3 in CR serum. To detect LC3I and LC3II bands, cells were preincubated as in **A**. (**E**) Quantitative analysis of the ratio of LC3II to LC3I ($n = 4$). (**F**) Hypoxia-induced autophagy in Bnip3-overexpressing cultured cells transfected with siRNA control or siRNA for Foxo3 in CR serum. Original magnification, ×400. Right: Percentage of GFP^+ cells with punctate GFP-LC3 fluorescence. Data are mean ± SEM. $^*P < 0.05$.

down-mediated inhibition of autophagy (Supplemental Figure 1), which suggests that Sirt1 positively regulates CR-mediated enhancement of hypoxia-induced autophagy upstream of Bnip3.

PI3K and Sirt1 regulate Foxo3 activity in the Bnip3 promoter. Since nuclear translocation of Foxo3 and its subsequent transcriptional activity are negatively regulated by PI3K-Akt–mediated phosphorylation (40), we next examined the role of PI3K and Sirt1 on Foxo3-mediated enhancement of hypoxia-induced Bnip3 expression in AL and CR serum. At the early stage of hypoxia (6 hours), Bnip3 expression was not detected in AL serum, whereas it was enhanced in CR serum (Figure 6A). At this stage, phosphorylated Foxo3 in AL serum showed cytoplasmic localization, and dephosphorylated Foxo3 in CR serum exhibited nuclear distribution (Figure 6, B and C). The PI3K inhibitor LY294002 in AL serum reversed phosphorylation of Foxo3 and enhanced its nuclear translocation (Figure 6, B and C). Because Sirt1 was localized in the nucleus in CR and AL serum (Figure 6B), we next investigated whether nuclear-translocated Foxo3 interacts with Sirt1. In AL serum, Foxo3 failed to interact with Sirt1 and was markedly acetylated even when it was translocated into the nucleus by LY294002 (Figure 6D). In contrast, under CR serum, nuclear Foxo3 interacted with Sirt1 and was deacetylated (Figure 6D). ChIP and IB revealed that acetylated

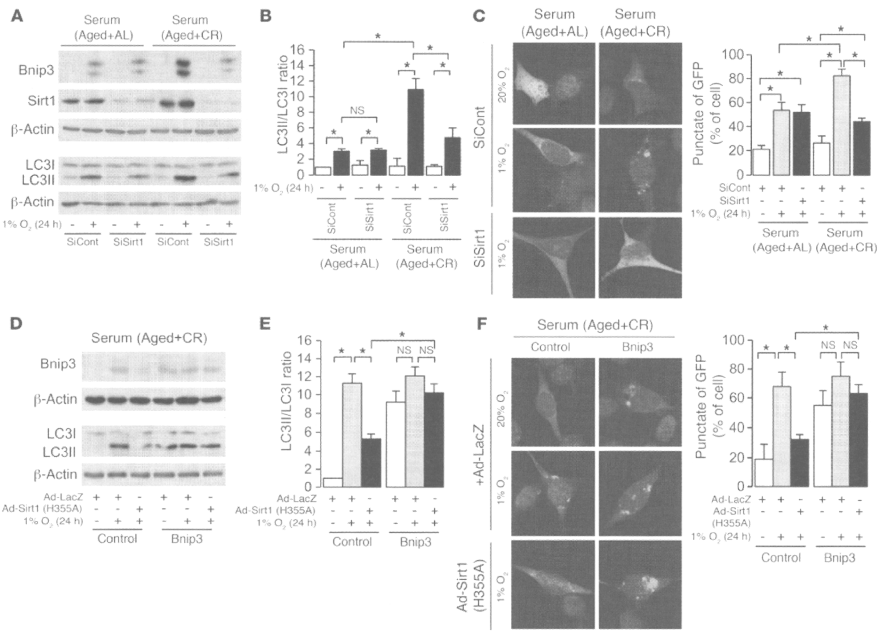

Figure 5

Involvement of Sirt1 in CR-mediated enhancement of autophagy under hypoxia. (**A**) Bnip3 and Sirt1 expression and LC3II formation in retrovirally mediated Sirt1-knockdown cells under hypoxia (1% O_2, 24 hours) in AL and CR serum conditions. To detect LC3I and LC3II bands, cells were preincubated with lysosomal inhibitor (E64d and pepstatin A). (**B**) Quantitative analysis of the ratio of LC3II to LC3I ($n = 4$). (**C**) Hypoxia-induced autophagy in Sirt1-knockdown cells under AL and CR serum conditions. Original magnification, ×400. Right: Percentage of GFP^+ cells with punctate GFP-LC3 fluorescence. (**D**) Expression of Bnip3 and LCII formation under hypoxia in retrovirally mediated Bnip3-overexpressing cells infected with either adenoviral mutated Sirt1 (H355A) or LacZ in CR serum. To detect LC3I and LC3II bands, cells were preincubated as in **A**. (**E**) Quantitative analysis of the ratio of LC3II to LC3I ($n = 4$). (**F**) Hypoxia-induced autophagy in retrovirally mediated Bnip3-overexpressing cells infected with either adenoviral mutated Sirt1 (H355A) or LacZ in CR serum. Original magnification, ×400. Right: Percentage of GFP^+ cells with punctate GFP-LC3 fluorescence. Data are mean ± SEM. $^*P < 0.05$.

Foxo3 in AL serum failed to bind to Bnip3 promoter or enhance Bnip3 expression, whereas deacetylated Foxo3 in CR serum bound to Bnip3 promoter and subsequently enhanced Bnip3 expression under hypoxia (Figure 6, C and E). These conditions did not affect hypoxia-mediated Hif1a expression (Figure 6C).

PI3K and Sirt1 regulate Foxo3-mediated cell adaptation to hypoxia. Foxo3 is also recognized as a cell cycle regulator (G_1 arrest) through p27Kip1 expression (41) and as a proapoptotic factor through Bim expression (37, 42) in response to certain stress conditions. At the late phase (12–24 hours), hypoxia caused apoptosis in AL serum, as determined by cleavage of both poly(ADP-ribose) polymerase (PARP) and caspase 3 (Figure 6A). In contrast, hypoxia in CR serum enhanced p27Kip1 expression as well as autophagy with Bnip3 overexpression (Figure 6A). Thus, we next examined the role of interaction among PI3K, Sirt1, and Foxo3 on p27Kip1 expression, autophagy, and apoptosis in the late phase (24 hours) of hypoxia. Prolonged hypoxia in AL serum partially translocated Foxo3 to the nucleus, and this effect was blocked by N-acetyl-cysteine (NAC), an antioxidant molecule (Figure 7, A and B). NAC also inhibited hypoxia-mediated apoptosis in AL serum (Figure 7B). In contrast, LY294002 increased Foxo3 nuclear translocation and apoptosis (Figure 7, A and B). These results suggest that oxidative stress–mediated nuclear translocation of Foxo3 causes apoptosis under hypoxia in AL serum, which is inhibited by PI3K. In CR serum, Foxo3 was localized in the nucleus under both normoxia and hypoxia (Figure 7, A and B), and Bnip3-mediated autophagy was enhanced under hypoxia (Figure 7, B and C).

Similar to the results of early phase, nuclear Foxo3 failed to interact with Sirt1 and was markedly acetylated in AL serum, whereas it interacted with Sirt1 and was deacetylated in CR serum (Figure 7D). ChIP and IB showed that acetylated Foxo3 in AL serum failed to bind to both Bnip3 and p27Kip1 promoters, and bound to Bim

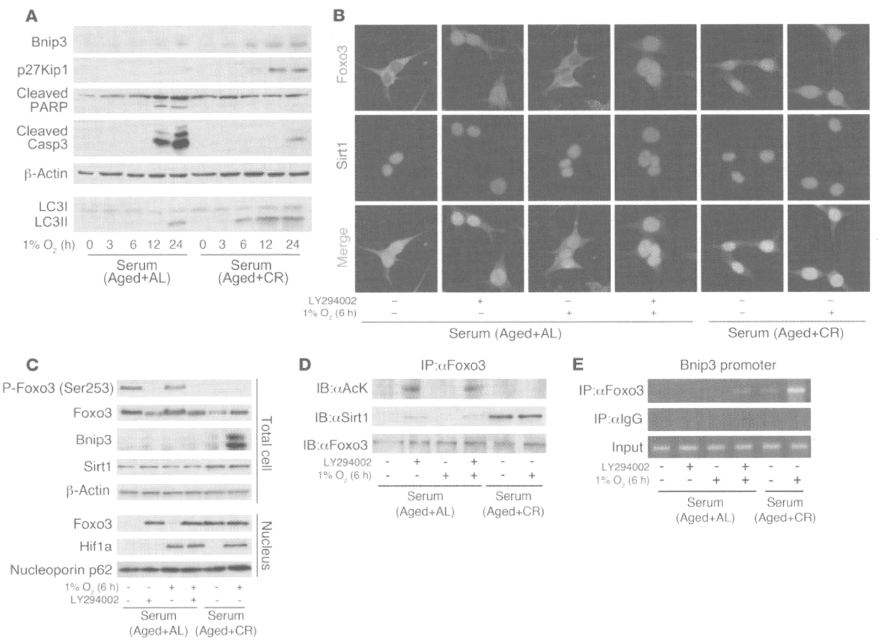

Figure 6

Involvement of PI3K and Sirt1 in Foxo3-mediated Bnip3 expression at early phase of hypoxia. (**A**) IB for Bnip3, p27Kip1, cleaved PARP, and cleaved caspase 3 expression and LC3II formation at the indicated time points under hypoxia (1% O_2) in AL and CR serum. To detect LC3I and LC3II bands, cells were preincubated with lysosomal inhibitor (E64d and pepstatin A). (**B**) Immunostaining showing localization of Foxo3 and Sirt1 at early phase of hypoxia (1% O_2, 6 hours) under the indicated conditions. Original magnification, ×400. (**C**) Phosphorylation and expression levels of Foxo3, expression levels of Bnip3 and Sirt1, and nuclear expression levels of Foxo3 and Hif1a at early phase of hypoxia. (**D**) Acetylation of Foxo3 and interaction between Sirt1 and Foxo3 at early phase of hypoxia. (**E**) ChIP analysis to determine Foxo3 binding to Bnip3 promoters at early phase of hypoxia. LY294002 was used as PI3K inhibitor at 20 μM.

promoter, in hypoxic PTCs (Figure 7E), which suppressed autophagy and p27Kip1 expression and increased apoptosis (Figure 7, B and C). LY294002 enhanced Foxo3 binding to Bim promoter under AL serum (Figure 7E). In contrast, deacetylated Foxo3 in CR serum bound to Bnip3 and p27Kip1 promoters, but not Bim promoters (Figure 7E), which mediated autophagy and p27Kip1 expression and suppressed apoptosis (Figure 7, B and C).

Retrovirally mediated Sirt1 knockdown in CR serum enhanced hypoxia-induced apoptosis and inhibited p27Kip1 expression and Bnip3-mediated autophagy (Figure 8, A and B). We next examined the mechanisms of these actions. Sirt1 deficiency in CR serum enhanced acetylation of Foxo3 (Figure 8C). Acetylated Foxo3 failed to bind to both Bnip3 and p27Kip1 promoter and bound to Bim promoter (Figure 8D). In contrast, Sirt1 overexpression in AL serum with LY294002 augmented Bnip3-mediated autophagy and p27Kip1 expression, decreased apoptosis (Figure 8, E and F), and increased Foxo3 binding to Bnip3 and p27Kip1 promoter (Figure 8G). Under the same conditions, siRNA for Foxo3 suppressed Sirt1-mediated enhancement of Bnip3-mediated autophagy and p27Kip1 expression (Figure 8, E and F), which suggests that Sirt1 promotes cellular adaptation to hypoxia through the regulation of transcriptional activity of Foxo3 to Bnip3, p27Kip1, and Bim.

CR fails to enhance cell adaptation to hypoxia in aged kidney of Sirt1$^{+/-}$ *mice.* We provided in vivo evidence for the involvement of Sirt1 in CR-mediated cellular adaptation to hypoxia by using 12-month-old *Sirt1*$^{+/-}$ mice on SV129 background under AL and CR for 6 months. The PTCs of 12-month-old WT mice showed normal mitochondrial morphology and little mitochondrial oxidative damage, together with substantial increases in autophagy and hypoxia-associated Bnip3 expression (Figure 9, A–G). In contrast, *Sirt1*$^{+/-}$ AL mice showed damaged mitochondria, higher levels of urinary 8-OHdG excretion, and higher prevalence of point mutation of mtDNA in the kidney; additionally, autophagy and Bnip3 expression in the hypoxic PTCs of *Sirt1*$^{+/-}$ AL mice were significantly

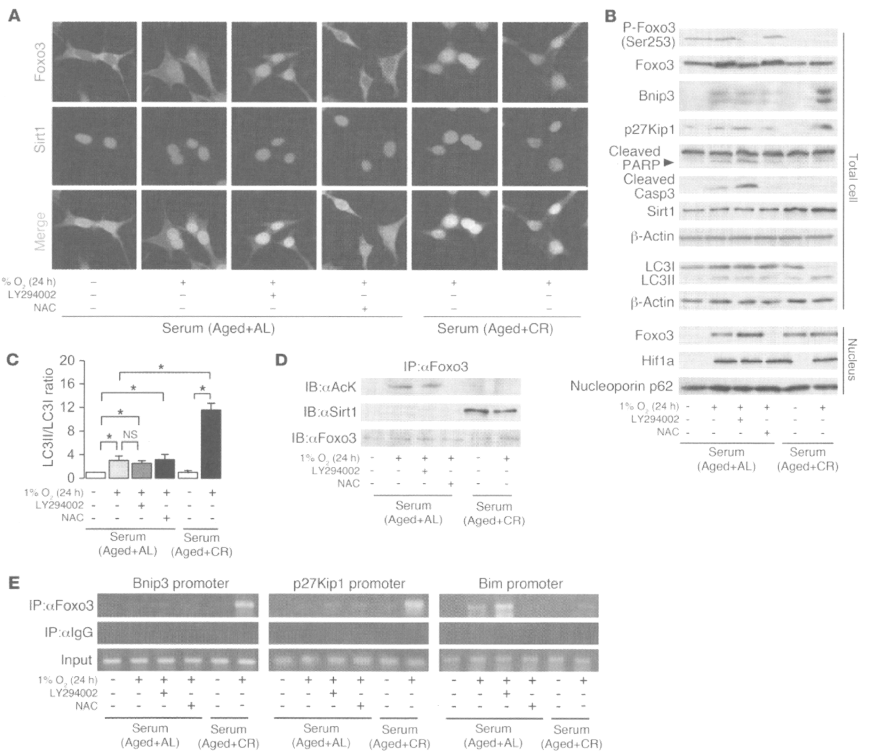

Figure 7

Involvement of PI3K and Sirt1 in Foxo3-mediated cell adaptation to hypoxia. (**A**) Immunostaining showing localization of Foxo3 and Sirt1 at late phase of hypoxia (1% O_2, 24 hours) under the indicated conditions. Original magnification, ×400. (**B**) Phosphorylation and expression level of Foxo3; expression of Bnip3, p27Kip1, cleaved PARP, cleaved caspase 3, and Sirt1; formation of LC3II; and nuclear expression levels of Foxo3 and Hif1a at late phase of hypoxia. To detect LC3I and LC3II bands, cells were preincubated with lysosomal inhibitor (E64d and pepstatin A). (**C**) Quantitative analysis of the ratio of LC3II to LC3I ($n = 4$). (**D**) Acetylation of Foxo3 and interaction between Sirt1 and Foxo3 at late phase of hypoxia. (**E**) ChIP analysis to determine Foxo3 binding to the promoters of Bnip3, p27Kip1, and Bim at late phase of hypoxia. LY294002 was used as a PI3K inhibitor at 20 μM. NAC was used as an antioxidant at 20 mM. Data are mean ± SEM. *$P < 0.05$.

decreased. CR failed to enhance hypoxia-induced Bnip3 expression and autophagy (Figure 9, D–G), which caused mitochondrial oxidative damage in the kidneys of *Sirt1*$^{+/-}$ mice (Figure 9, A–C), although they showed the systemic phenotype of CR mice (Supplemental Table 2). These results suggest that Sirt1 in the kidney is essential for the CR-mediated enhancement of hypoxia-associated mitochondria oxidative damage in vivo. We also confirmed that the phenotypes of aged kidneys of 12-month-old WT, *Sirt1*$^{+/-}$ AL, and *Sirt1*$^{+/-}$ CR mice of C57BL/6 background were similar (Supplemental Figure 2, A and B) to those of mice of SV129 background (Figure 9, A and D), which suggests that the difference in genetic background does not affect the role of Sirt1 in hypoxia-associated mitochondrial damage and cellular adaptation in the kidney.

In the kidneys of WT mice, Foxo3 interacted with Sirt1 and was deacetylated, whereas its acetylation was enhanced in *Sirt1*$^{+/-}$ mice with both AL and CR (Figure 9H). In agreement with the results of the in vitro study, deacetylated Foxo3 bound to Bnip3 and p27Kip1 promoters (Figure 9I), resulting in increased expression levels of these proteins in WT mice (Figure 9D). In contrast, acetylated Foxo3 in the kidneys of *Sirt1*$^{+/-}$ AL and CR mice failed to bind Bnip3 and p27Kip1 promoters (Figure 9I), and their expressions subsequently decreased (Figure 9D). Furthermore, Foxo3 binding to Bim pro-

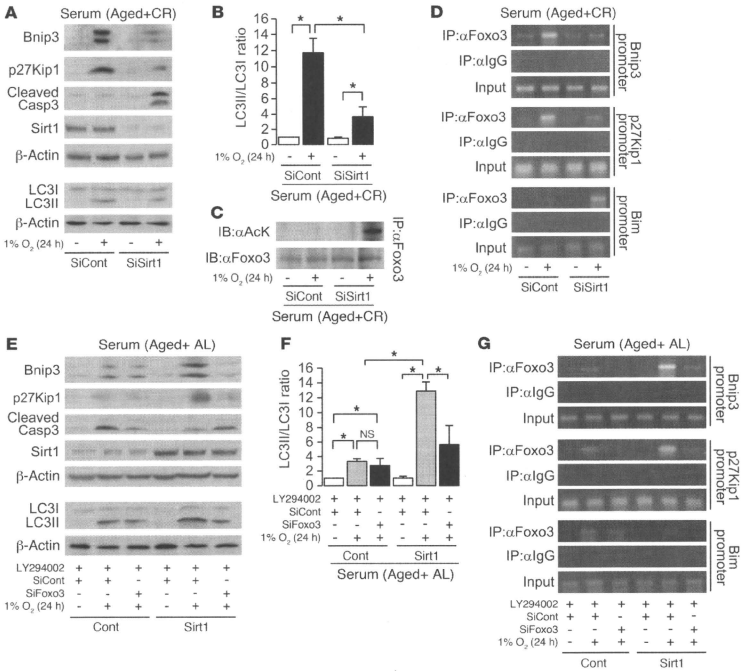

Figure 8

Role of Sirt1 in cell adaptation to hypoxia. (**A**) Expression levels of Bnip3, p27Kip1, cleaved caspase 3, and Sirt1 and formation of LC3II in retrovirally mediated Sirt1-knockdown cells under hypoxia (1% O_2, 24 hours) in CR serum condition. To detect LC3I and LC3II bands, cells were preincubated with lysosomal inhibitor (E64d and pepstatin A). (**B**) Quantitative analysis of the ratio of LC3II to LC3I ($n = 4$). (**C**) Acetylation of Foxo3 in Sirt1-knockdown cells under hypoxia in CR serum. (**D**) ChIP analysis to determine Foxo3 binding to promoters of Bnip3, p27Kip1, and Bim in Sirt1-knockdown cells under hypoxia in CR serum. (**E**) Expression levels of Bnip3, p27Kip1, cleaved caspase 3, and Sirt1 and formation of LC3II in retrovirally mediated Sirt1-overexpressing cells transfected with siRNA control or siRNA for Foxo3 under hypoxia in AL serum. To detect LC3I and LC3II bands, cells were preincubated as in **A**. (**F**) Quantitative analysis of the ratio of LC3II to LC3I ($n = 4$). (**G**) ChIP analysis to determine Foxo3 binding to promoters of Bnip3, p27Kip1, and Bim in Sirt1-overexpressing cells transfected with siRNA control or siRNA for Foxo3 under hypoxia in AL serum. LY294002 was used as a PI3K inhibitor at 20 μM. Data are mean ± SEM. $^*P < 0.05$.

moter (Figure 9I) and subsequent cleavage of caspase 3 (Figure 9D) were enhanced in the kidneys of *Sirt1*$^{+/-}$ AL and CR mice. Finally, serum cystatin C levels were significantly higher in *Sirt1*$^{+/-}$ AL mice, and were not attenuated by 6 months of CR (Figure 9J).

Discussion

Our results provided the first evidence to our knowledge that long-term CR enhances autophagy with overexpression of Sirt1 in aged tissue of mammals and is a therapeutic target for age- and hypoxia-associated tissue damage including aged kidney. In this study, we focused on Sirt1, a survival molecule under CR (23, 24, 43, 44). Recent reports suggest that *Sirt1* transgenic mice show a phenotype that resembles mice under CR (45), and *Sirt1* deficiency in mice failed to show lifespan prolongation under CR (46). However, few studies have provided direct evidence for the involvement of Sirt1 in the pathogenesis of age-associated mitochondrial damage or in the mechanism underlying long-term CR-mediated mitochondrial protection. In the present study, Sirt1 expression was significantly decreased in aged kidney and was enhanced by long-term CR. Furthermore, the results showing acetylation state of Foxo3 emphasized the suppression of Sirt1 deacetylase activity in aged kidney and its enhancement by long-term CR. We believe we are the first to show that long-term CR can cause Sirt1 activation even in aged tissues.

The in vitro model of CR has been used to determine the effects of CR serum on cell proliferation (39), apoptosis (38), and mitochondria biogenesis (20). Using this model, we showed that aging AL and CR serum affected hypoxia-induced autophagy through modification of the Sirt1-PI3K-Foxo3 axis. Sirt1 deficiency and

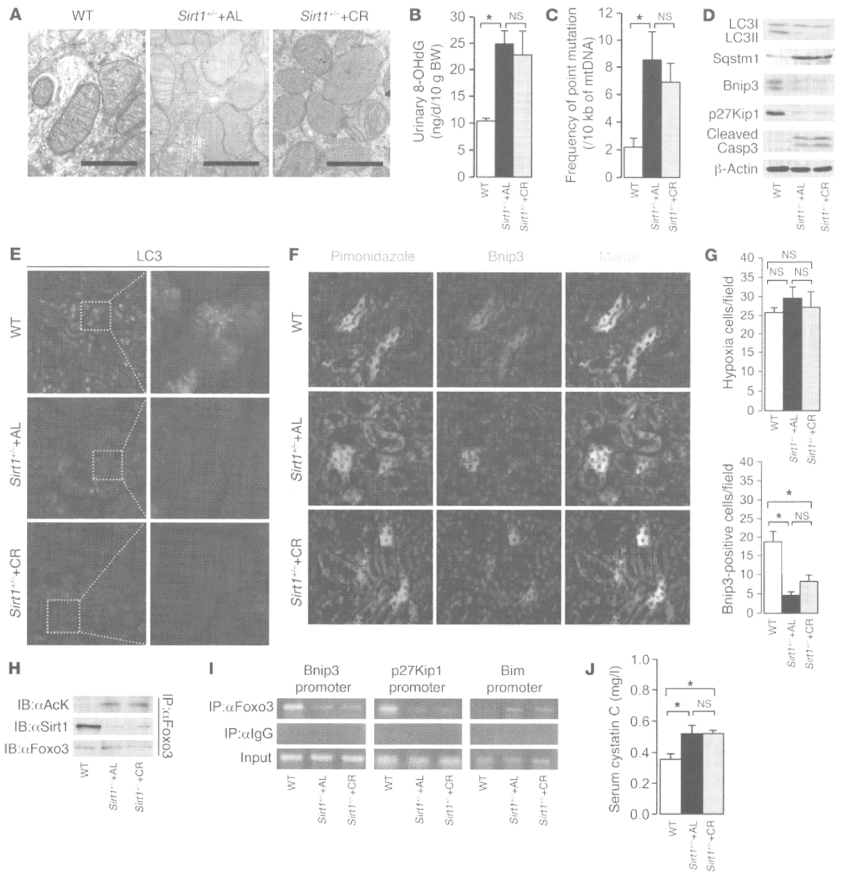

Figure 9

Effect of CR on Foxo3-mediated cell adaptation in the kidneys of aged *Sirt1*$^{+/-}$ mice. We examined 12-month-old WT mice, *Sirt1*$^{+/-}$ AL mice, and *Sirt1*$^{+/-}$ mice on CR for 6 months. (**A**) EM of a renal PTC. Scale bars: 1 μm. (**B**) Urinary 8-OHdG excretion. (**C**) Frequency of point mutation of mtDNA in the kidney. (**D**) LC3II formation and expression levels of Sqstm1, Bnip3, p27Kip1, and cleaved caspase 3 in the kidney. (**E**) Immunofluorescence study for LC3 protein in the kidney. Original magnification, ×400 (left); ×1,000 (right). (**F**) Immunofluorescence study for pimonidazole and Bnip3 in a kidney section. Original magnification, ×400. (**G**) Quantitative analysis of hypoxic pimonidazole$^+$ and Bnip3$^+$ cells per field in the kidney. (**H**) Acetylation of Foxo3 and interaction between Sirt1 and Foxo3 in the kidney. (**I**) ChIP analysis to determine Foxo3 binding to the binding site in the Bnip3, p27Kip1, and Bim promoters in the kidney. (**J**) Serum cystatin C levels at the end of experimental periods. Data are mean ± SEM. **P* < 0.05. Each group includes 5–7 mice.

enhanced PI3K during the aging process suppress both autophagy and cell cycle arrest even under hypoxic conditions, which results in accumulation of oxidative stress and subsequent apoptosis through acetylated Foxo3-mediated Bim expression (Figure 10A). In contrast, CR-mediated Sirt1 activation promotes cell adaptation to hypoxia through Bnip3-mediated autophagy and p27Kip1 expression via deacetylation of Foxo3 (Figure 10B). Furthermore, the results of in vivo study showing the effect of CR on age-associated kidney phenotypes in *Sirt1*$^{+/-}$ mice were in agreement with this molecular mechanism. Our present results provide insight into the molecu-